Multi-Constriction Microfluidic Sensors for Single-Cell Biophysical Characterization

Parham Ghassemi

Thesis submitted to the faculty of the
Virginia Polytechnic Institute and State University
in partial fulfillment of the requirements for the degree of

Master of Science
In
Electrical Engineering

Masoud Agah, Chair
Wei Zhou
Yizheng Zhu

August 11th, 2017
Blacksburg, Virginia

Keywords: Microelectromechanical Systems(MEMS), microfluidics, impedance spectroscopy, cell deformability, cancer cells

Multi-Constriction Microfluidic Sensors for Single-Cell Biophysical Characterization

Parham Ghassemi

ABSTRACT

Cancer is a major health issue that has been associated with over 80 million deaths worldwide in the last decade. Recently, significant improvements have been made in terms of treatment and diagnosis. However, despite these advancements there is still a demand for low-cost, high-accuracy, and easy-to-use technologies capable of classifying cells. Analysis of cell behavior in microfluidic deformability assays provides a label-free method of observing cell response to physical and chemical stimuli. This body of work shows advancements made toward reaching our goal of a robust and cost-effective biosensing device that allows for the identification of normal and cancer cells. These devices can also monitor cell responses to physical and chemical stimuli in the form of mechanical deformation and chemotherapeutic drugs, respectively. Our initial design was a microfluidic device that consisted of three channels with varying deformation and relaxation regions. Cell velocities from the deformations regions allowed us to distinguish between normal and cancer cells at the single-cell level. The next design used a singular deformation channel that was embedded with an array of electrodes in order to measure entry time, transit time and velocities as a single cell passes through the channel. These factors were found to reveal information about the biomechanical properties of single cells. Embedded electrodes were implemented in order to reduce post processing times of the data analysis and provide more insight into the bioelectrical information of cells. Finally, we report a microfluidic device with parallel deformation channels and a single electrode pair to improve throughput and automate data collection of deformability assays. This thesis demonstrates how microfluidic deformability assays, with and without embedded electrodes, show promising capabilities to classify different

cells based on their biophysical traits which can be utilized as a valuable tool for testing responses to physical and chemical stimuli.

Multi-Constriction Microfluidic Sensors for Single-Cell Biophysical Characterization

Parham Ghassemi

GENERAL AUDIENCE ABSTRACT

Cancer is a worldwide health issue with approximately 1.7 million new cases each year in the United State alone. Although a great amount of research has been conducted in this field, the numerous uncertainties and heterogeneity among tumors, which is amplified by the large diversity between patients, has limit progress in both diagnostics and therapy. Traditionally, cancer studies have primarily focused on biological and chemical techniques. However, more recently, researchers have begun to leverage engineering techniques to acquire a new perspective on cancer to better understand the underlying biophysical attributes. Thus far, various engineering methodologies have produced meaningful results, but these techniques are costly and tend to be laborious. As a result, there is a need for low-cost, high-accuracy, and easy-to-use technologies to aid with cancer research, diagnostics, and treatment. An emerging field to alleviate these concerns is microfluidics, which is a science involving the flow of fluids in micro-scale channels. The field of microfluidics shows a great deal of promise for the development of clinically ready devices for analyzing cancer cells at both the population and single cell levels. Investigating the behavior of cancer cells at a single cell level can provide valuable information to help better understand the responsiveness of tumors to physical or chemical stimuli, such as chemotherapeutic drugs. This thesis reports multiple robust and cost-effective biomedical micro-devices that are used to analyze normal and cancerous cells. These devices consist of a microfluidic channel with sensors and are created using micro-fabrication techniques. The unique designs have enabled the evaluation of cells based on their mechanical and electrical properties. Specifically, the mechanical properties can be measured by forcing a cell into a microfluidic channel that is smaller than the diameter of the cell and recording its response to this physical stimulus. Electrical properties are measured

simultaneously as the cells are probed for their mechanical properties. In general, the mechanical and electrical properties of cells can be altered when they undergo internal change (i.e. diseased cells) or experience external stimuli. Thus, these properties can be utilized as indicators of cancer progression and can be used to distinguish tumorigenic from non-tumorigenic cells. Data collection from these devices is automated, allowing for the rapid acquisition of mechanical and electrical properties of cells with minimal post-processing. Results from these devices have been promising in their ability to indicate significant differences among various normal and cancer populations based on their mechanical and electrical attributes.

To my parents Farshid and Nazila…

Acknowledgments

I would first like to thank my academic and research advisor Dr. Masoud Agah, director of the VT MEMS Laboratory at Virginia Tech, for giving me the opportunity to work on these projects. His advice and guidance has helped me grow as a researcher and person. Next, I would like to express gratitude to Dr. Jeannine Strobl for her valuable input on my research and for helping me better understand the bio-related aspects of my work. Don Leber also deserves an acknowledgement for his assistance and advice in the cleanroom. I would also like to thank Dr. Wei Zhou and Dr. Yizheng Zhu for agreeing to be in my committee.

I am grateful for the previous and current members of the VT MEMS Lab who have helped me in the past two years including: Vaishnavi, Hesam, Xiang, Kru, Sepeedah, Sarah, Ana, and Ryan. I would like to give a special thanks to my labmate and mentor Dr. Xiang Ren, whose intricate approach to research and deep knowledge has motivated me to become a better researcher. I would also like to thank all my friends who have supported me and made life enjoyable.

Last but not least, I'd like to thank my parents, Dr. Farshid Ghassemi and Dr. Nazila Tehrani, and my siblings Pedram and Pegah for being my role models in life. Without them, I would not be where I am today academically and as a person.

Table of Contents

List of Figures

List of Tables

1. Introduction

Cancer is one of the leading causes of death in the world and is involved in approximately 9 million deaths each year, making it a major worldwide health problem [1]. Metastasis, the spread of cancer to other regions of the body via blood and lymphatic vessels, is the main cause of deaths due to cancer [2, 3]. Researchers across the world attempt to combat cancer by developing new techniques for early detection, screening, treatment, and improving quality of life [1, 4, 5]. However, early detection, screening, and treatment can be difficult because of the heterogeneity of cancer from patient to patient. In fact, the underlying mechanisms which cause the formation and progression of cancer cells still remains largely unknown. Thus, understanding the biophysical properties of cells can help create a connection between the mechanics and biological functions of cells [6, 7].

In order to improve our insight on these biophysical properties, we developed microfluidic biosensing devices capable of revealing information about the biomechanical and bioelectrical properties of single cells. Using this information, we were able to differentiate between normal and cancer cells, as well as test the effects of chemotherapeutic drugs on such biophysical properties. In this chapter, we will examine cells modeled as mechanical and electrical objects in combination with current microfluidic platforms that combine deformability assays and impedance spectroscopy.

1.1 Cell as a Mechanical Object

A cell mainly consists of three important components: membrane, cytoskeleton, and nucleus (Figure 1.1) [8].The cytoskeleton is the structural foundation of a cell that defines the shape of the cell and plays a key role in its mechanical rigidity [9]. The cell cytoskeleton consists

of three different kinds of protein filaments (shown in Figure 1.2): actin filaments (or microfilaments), intermediate filaments, and microtubules [10, 11].

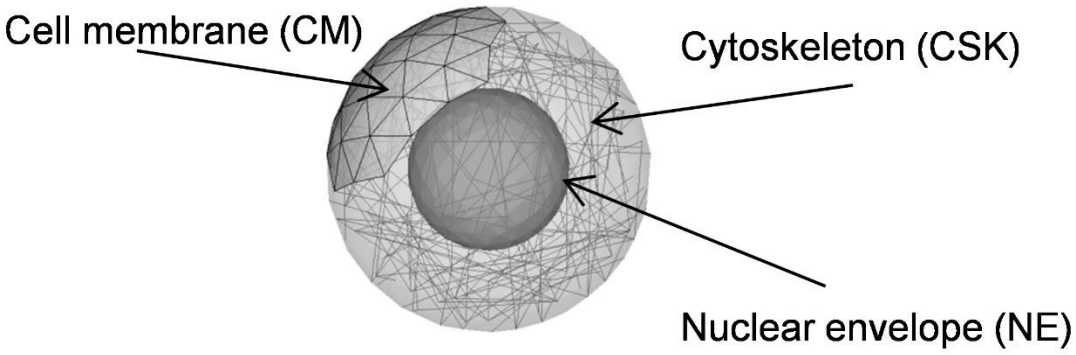

Figure 1.1: Overview of main cell components [8].

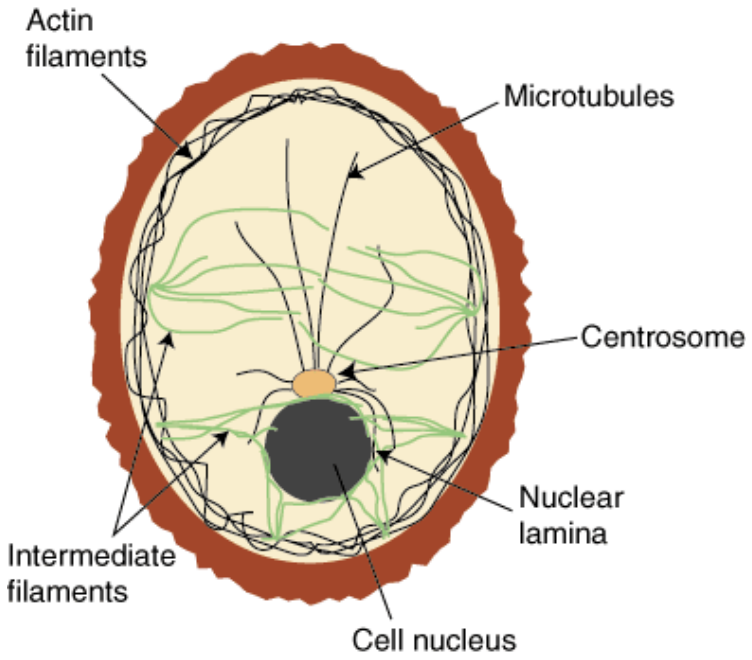

Figure 1.2: Illustration of cell with cytoskeleton components [12].

Microtubules provide the basic organization of the cytoplasm, actin filaments contribute to cell shape and are involved in cytokinesis and cell movement, and intermediate filaments provide

mechanical support for the plasma membrane [10, 13]. In general, actin filaments play a vital role in the structural integrity and deformability of the cell when it experiences lower strains. In contrast, intermediate filaments tend to deform only when the cell experiences larger strains. Microtubules are primarily responsible for providing structure to the cytoskeleton [13]. One model used to describe the role of actin filaments and microtubules is the Tensegrity Model.

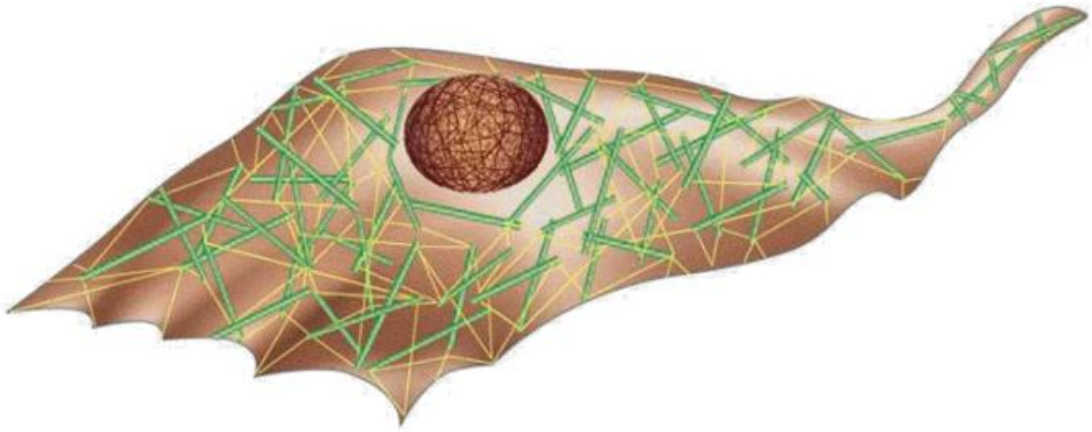

Figure 1.3: A cell and its contractile filaments and compressive elements [14].

The Tensegrity (tensional integrity) model is a method of evaluating the structure of a cell and understanding the mechanics of its behavior. The model suggests that cell structure and shape relies on preexisting tensile stresses (prestresses) in the cytoskeleton. The fibers in the cytoskeleton, primarily actin filaments, behave like muscles and create tension [15-20]. These prestresses are balanced by the internal compression from cytoskeletal components (microtubules) and adhesion forces from the extracellular matrix [18, 21]. The mechanical rigidity and stiffness of cells are correlated to these preexisting stresses, suggesting that more prestress indicates more stability and lower deformability [15-20]. Figure 1.3 illustrates a cell with prestress filaments and compressive stress elements [14]. The yellow lines are the prestress filaments and the green tube-like structures are the compressive stress elements. Cell characterization can be then done by using

biomechanical properties of the cells, such as size and deformability [22]. These characteristics can help define the metastatic potential of cells.

Cancer cell metastasis depends on its ability to deform into blood and lymphatic vessels [3]. Cell deformability can operate as a potential biomarker to differentiate diseased and healthy cells [22-25]. Benign and cancerous cells have differences in stiffness, as it is well known that cancer cells are more deformable than normal cells [22-26]. Single-cell deformability can also be used as a label-free biomarker for cell phenotyping and assessing cancer invasiveness [22]. Single-cells passing through deformation regions is used as a method to test the deformability of cells. Deformation regions are microfluidic channels that have cross-sections smaller than the cell's diameter, which essentially force the cells to deform in order to pass through the channel. The time it takes for cells to enter (entry time) and pass through (transit time) the deformation channel can be used to characterize the cells.

Cell stiffness is related to invasiveness and researchers have used these mechanical phenotypes as targets for molecular therapy of cancer. Cells that are more invasive tend to have softer mechanical characteristics, which improves its ability to deform like those in a metastatic population [27]. When comparing similarly sized cells with different metastatic potential, higher metastatic potential correlates to faster entry times in a deformability channel than cells with lower metastatic potential. Also, cells with higher metastatic potential show increases in transit times. This suggests that not only does deformability increase, but friction is possibly reduced, which could play a role in invasive cancer cells squeezing into tight spaces [28]. In general, cancer cells are associated with increasing deformability when compared to normal epithelial cells [22, 23, 25, 29].

Current developed methods for cell deformability and cell elasticity measurements include: micropipette aspiration [30-32], atomic force microscopy [33-35], optical deformability [23], magnetic bead twisting assays [36], and optical tweezers [37].

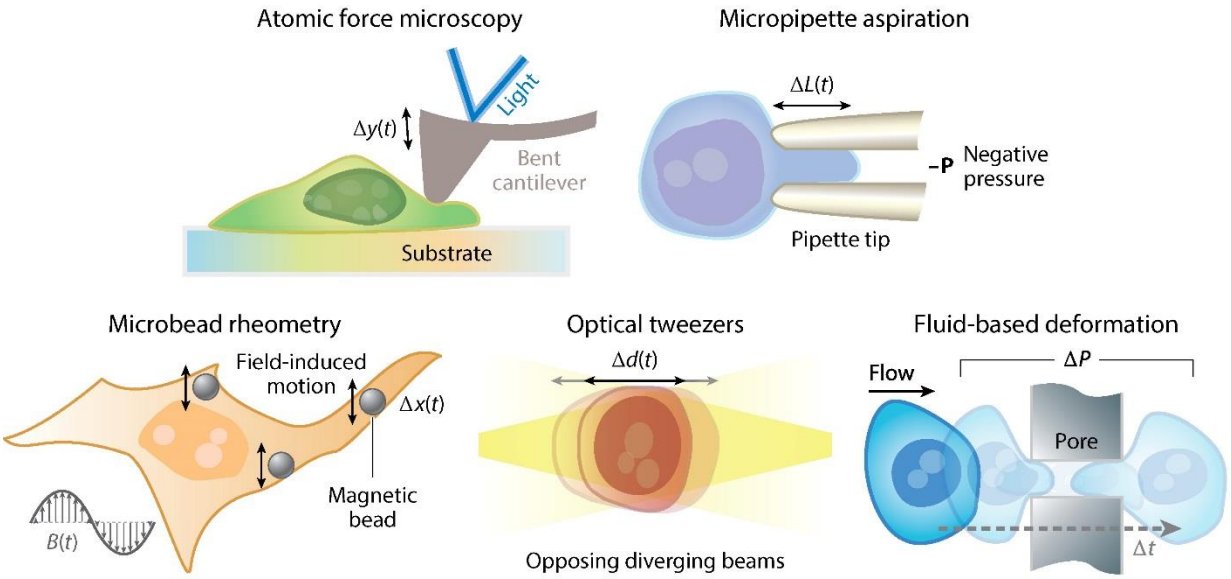

Figure 1.4: Traditional techniques used to measure mechanical properties of cells [38].

AFM is used as a method to look at cells by probing the sample with a cantilever tip to study its mechanical properties. Studies show that using AFM, relative metastatic potential of ovarian(and possibly other types of cancer cells) can by evaluated by using cell stiffness as a biomarker [39]. There are many issues involved with AFM, including extensive sample preparation, low repeatability, experimental costs, and unrealistic cell environment.

Another method of probing cell deformability is through a dual beam optical stretcher [23, 26]. Using the optical stretcher technique it was realized that cancer cells deforms 5X more than normal cells and metastatic cells deform 2X more than non-metastatic cancer cells [26]. The issue with optical stretching techniques is that forces applied on the cell from a laser is not sufficient to

completely deform the cell and is not good for simulating in vivo conditions of cell migration [24]. Dual beam optical stretchers have been improved by incorporating a microfluidic cell delivery system to look at cell biomechanical properties in a more realistic environment. By looking at the cell's response to constant stress, it was discovered that cancer cells experience higher axial strain than normal cells [25]. By utilizing a magnetic tweezer system, the mechanical stiffness of cells with varying invasiveness were compared. It was discovered that cancer cells with the lowest migratory and invasive potential are 5X stiffer than their highest migratory and invasive potential counterparts. This proves that mechanical phenotypes can be key component for determining metastatic potential of cell populations and even at the single-cell level [27].

The main disadvantages of using these techniques is that they have low throughputs [22]. To overcome this issue, researchers are looking to also improve robustness and ease-of-use of these platforms [7]. To improve the throughput of cell classification using mechanical deformability, a method that involves using deformability induced forces and inertial lift forces in inertial microfluidic platforms [22]. These devices take advantage of micro-scale scale phenomena to provide a high-throughput platform for cell classification using cell deformability as a biomarker. Recently, Hydrodynamic stretching of single cells [40] and microcavity arrays [41] have also be used in high-throughput mechanical phenotyping [40, 41]. These devices have been proven to be useful for cell separation and high-throughput deformability measurements [22]. Although the throughput issue was addressed, long post-processing times and complexity of usage still exists.

Microfluidic deformability cytometry provides comparable statistical accuracies to traditional flow cytometry techniques, and also uses label-free biophysical biomarkers, opening opportunities for clinical diagnosis, stem cell characteristics and single-cell biophysics [40].

To conclude, cell deformability in microfluidics platforms can be used as a biomarker for identifying cells of different malignancies from a sample which proves that it is capable of being used in cancer diagnostic applications [24].

1.2 Cell as an Electrical Object

Single cells can be modeled as a dielectric shell, where each layer has its own permittivity and conductivity. The simplest model is the single-shell model, shown in Figure 1.5, which is useful for representing nucleus-free cells such as a red blood cell. The multi-shell model, shown in Figure 1.6, adds complexity to the model but better represents nucleated cells [42]. For example looking at the double shell model shown in Figure 1.7, starting from the inner to outer region the model represents the cell nucleus, nuclear envelope, cytoplasm, and plasma membrane, respectively. Each region also has its own respective dielectric properties such as permittivity and conductivity [43].

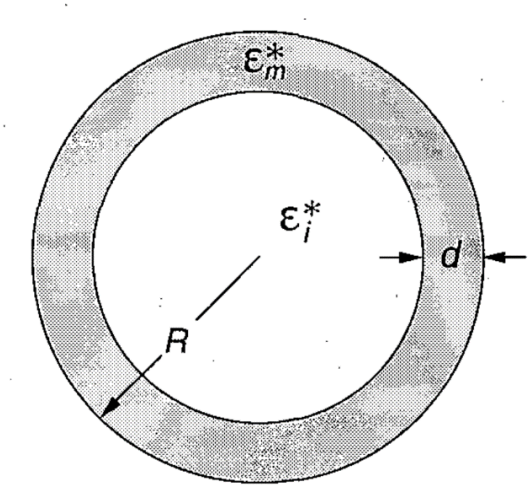

Figure 1.5: Single-shell model of cell [42].

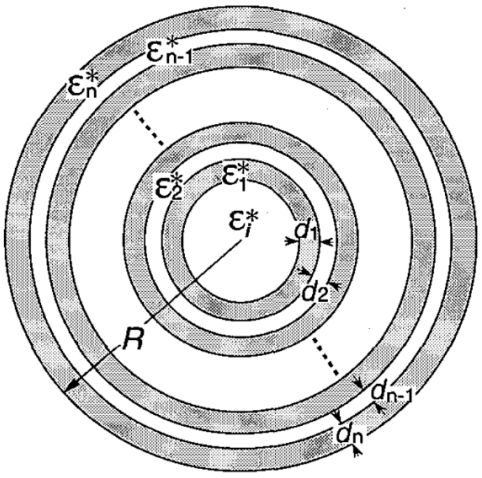

Figure 1.6: Multi-shell model of cell [42].

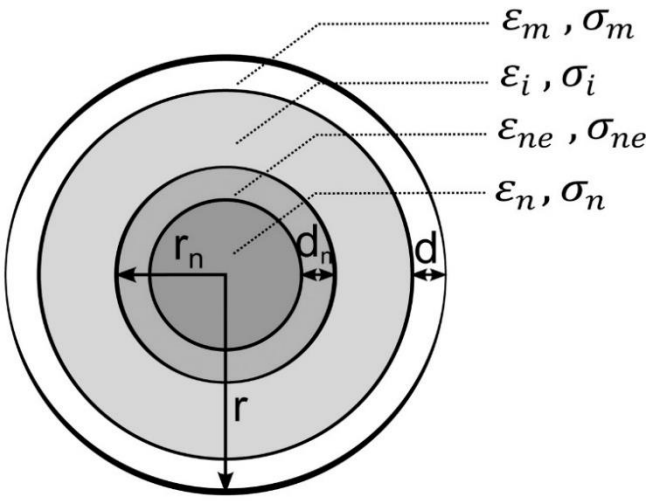

Figure 1.7: Double-shell model of a cell with corresponding dielectric and geometric parameters [43].

Impedance spectroscopy techniques can be used to measure the dielectric properties of single cells which can be modeled as a combination of linear components, such as a resistor and/or capacitor, in an electric circuit model (Figure 1.8) [44]. These electrical components can represent cell membrane resistance and capacitance, along with cytoplasm resistance.

Impedance spectroscopy can be used to obtain physiological properties from cells and has advantages that include simplicity, ease of use, non-invasive, and real-time capabilities. When an AC signal passes through the cell has a low frequency, the plasma membrane will act a barrier to the flow of current, which can be measured as an impedance value. The impedance value has an amplitude and phase that is proportional to the cell's volume. At higher frequencies, the membrane is permeable to the electrical AC current and the measurements provide information about the intracellular contents. At intermediate frequencies the membrane acts less like a barrier and can provide information about the properties of the cell membrane. The current flow passing through cells at difference frequencies is shown in Figure 1.9. Different frequencies can provide different information about the cell, therefore multi-frequency measurements provide the capability to distinguish cells by size, membrane properties, and intracellular properties [45].

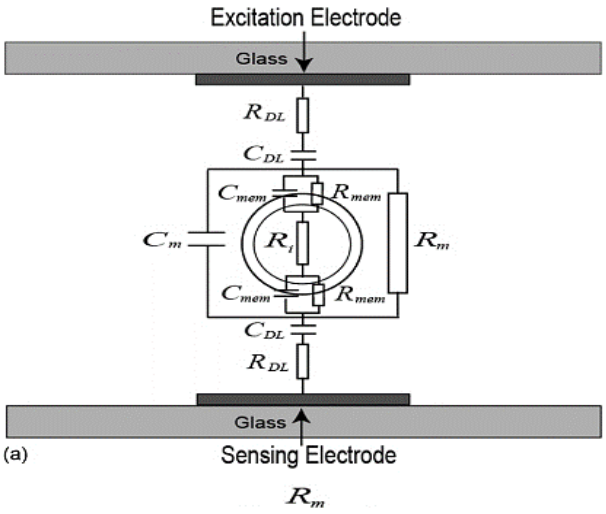

Figure 1.8: Electric circuit model for cell suspended between a pair of electrodes [44].

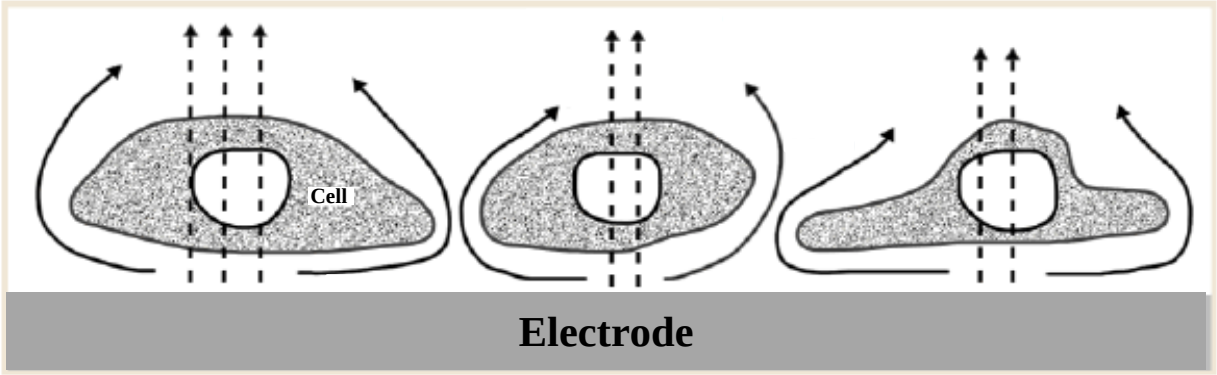

Figure 1.9: Diagram of current flow through cells at low (solid lines) and high frequencies (dotted lines) [46].

There are a variety of impedance spectroscopy techniques that can be used to extract these electrical properties of cells and cell populations. These techniques include Electrical Cell-Substrate Impedance Sensing (ECIS) and impedance spectroscopy in flow cytometry. ECIS involves measuring the change of the impedance of an electrode or across an electrode pair as an AC current passes through it. This technique is used to monitor the dynamic changes of biological cells that have adhered onto the typically gold electrodes. ECIS relies on the cells' ability to resist

the flow of electric current and measurements can be taken at singular frequencies or a sweep across multiple frequencies[47]. The impedance is directly related to the adherence of the cells onto the electrodes, so it can be used to measure cell growth and proliferation. As cells begin to die the impedance will decrease because they will detach from the electrode surface. Due to this cellular behavior, other applications for ECIS device include measuring responses to chemical stimuli, which can be useful for evaluating the cytotoxicity of drugs and screening for optimal drug dosage in treatments. Although ECIS can be used in a wide variety of applications, it has restrictions due to its reliance on cell adherence. This technique is not suitable for single-cell analysis, but other methods such as impedance spectroscopy in flow cytometry have that capability. Impedance spectroscopy in flow cytometry can also have a high-throughput, making it applicable for cell population studies as well.

Impedance spectroscopy in flow cytometry can be a tool for label-free cell characterization. Cell characterization is done by finding cell size, membrane capacitance, and cytoplasm conductivity as a function of frequency [48]. Dielectric spectroscopy has the potential to be used in the following applications: cell differentiation, mitosis/cell cycle monitoring, cytotoxicity and cell death, and as a drug screening platform. Cell differentiation is characterized by changes in cell morphology, aggregation, cell adhesion, ion channel activity or gene and protein expression, which are all changes that result in changes in the impedance spectrum of the cell [45].

Impedance spectroscopy in flow cytometry has also been used as a label-free method for quantifying the progression of cancer cells. Researchers have compared normal breast epithelial cells (MCF10A) to early stage breast cancer cell line (MCF-7), invasive human breast cancer cell line (MDA-MB-231), and metastasized human breast cancer cell line (MDA-MB-435). It was shown that the magnitude and phase had convincing differences from the cancer cell lines. This

device could lead to development of diagnostic tools for cancer detection and drug therapy [49]. Wide microfluidic channels have been used to measure electrical properties of single cells and model the cell as an equivalent circuit. Using this model, they interpret the data measured at various frequencies in order to find cell cytoplasm conductivity and specific membrane capacitance [50]. Another application of impedance flow cytometry is pollen analysis where the robust and label-free method can provide reliable data estimating plant cell viability [51].

Impedance measurements can also be a viable non-invasive method to monitor cells during mitosis and their cell cycle. Dying cells experience change in impedance and can be used to measure the effect of chemicals on cell mortality [45]. Additionally, flow cytometry combined with impedance measurements have been used to discriminate between live and dead cells [52]. Impedance also has a great deal of potential to screen for the cytotoxicity of various agents, including chemicals, drugs, and florescent tags and can also observe the stresses these reagents have on the cells. This technology can be implemented in point-of-care systems which can act as a biosensor for quick real-time measurements, replacing traditionally slow and invasive cytotoxicity assays [45]. Drug concentrations and drug incubation time have shown to have an inversely proportional effect on cell impedance values [53-56]. These systems can also have high-throughput due to their multiplexing capabilities. Therefore, these platforms have the ability to test different drugs and drug dosages in the same conditions simultaneously [45].

To conclude, impedance spectroscopy is a valuable tool in cell biosensing applications and there is great potential as a cost effective tool to replace conventional methods of cell analysis. Traditionally, extensive sample prep could include staining, labeling, and fixing of samples, all of which can be replaced using this label-free method. Impedance spectroscopy can be used in label-free analyzers for applications including: cell differentiation, cell cycle progression, cytotoxicity,

and cell death detection. Implementation into microfluidic systems allows for the flexibility of devices to be incorporated into systems for cell monitoring, drug screening, flow cytometry and even point-of-care platforms. Impedance spectroscopy allows label-free, rapid, cost-effective and highly sensitive technique that holds great potential in becoming a standard in biological cell characterization for a wide array of applications [45].

1.3 Microfluidic Approach to deformability assays and impedance Spectroscopy

Microfluidics have been used to look at the behavior of breast cancer cells and have the ability to distinguish between non-malignant and malignant cells. The benefits of microfluidics includes the ability to study over the overall cell mechanical properties and they can better mimic in vivo conditions that the cells will experience [24]. Biomechanical properties of cells obtained in deformability assays can give information on cell health, for example cell stiffness changes when cells change from a healthy to unhealthy state [57]. Entry time and transit time can be used to distinguish between non-malignant and malignant cells. For example, when comparing normal and cancer breast cells, transit times of both are approximately equivalent but normal cells have much higher entry times [24]. Impedance measurements from frequencies 40 Hz to 1 GHz supply information about membrane capacitance, cytoplasm conductivity and cytoplasm permittivity as a function of frequency. Multi-frequency measurements applied to a single cell can give us ability to classify a cell by size, membrane properties, and intracellular properties [58].

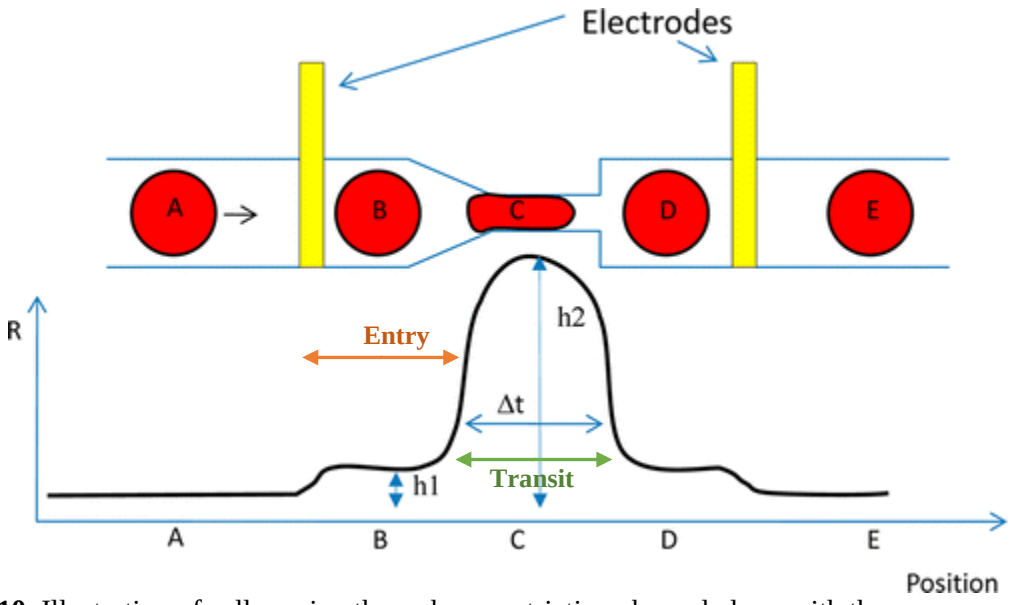

Figure 1.10: Illustration of cell passing through a constriction channel along with the corresponding impedance plot [57].

Electrodes imbedded in a microfluidic device with a deformability channel enhances throughput and heavily reduces post-processing, which is shown below in Figure 1.10 [57]. Researchers have developed a device that monitors cell during the cell cycle and can detect the transition between different physiological states [59]. During the cell cycle (Figure 1.11), cell impedance increases while cell duplicates its contents and during DNA replication (G1 and S phase). In contrast, impedance decreases during mitosis (nuclear division) and cell division (G2 and M phases) [60]. These types of devices can be used as tools for cell cycle studies.

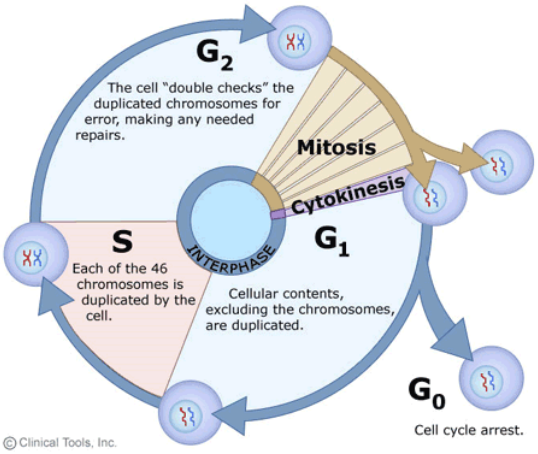

Figure 1.11: Description of the cell cycle [61].

Currently, one technique that combines impedance measurements in microfluidic deformability assays use micropillar traps to capture the cells and take impedance measurements [62, 63]. To improve impedance measurements, carbon nanotubes are being used as biosensors for cancer metastatic diagnosis with single-cell resolution. This tool was used for distinguishing cancerous stages of both breast and colon carcinoma cells [62]. Further research is being done for real-time monitoring of cells. In one case, cells' electrical responses have been measured during mechanical aspiration. This system was used for comparing healthy cells to malignant ones in real-time. Results also showed that the remodeling of actin filaments decreased their electrical response and cancer cells did not change as much as healthy cells [63].

Previously at the VT MEMS Lab, others investigated mechanical response of cells using AFM [64]. It was shown that cancer cells with high metastatic potential are softer than their non-invasive counterpart. As an extension of that study, in order to replace the need of the high-costing and unrealistic deformation conditions, a microfluidic deformability assay was developed with a single deformation channel [65]. Another device was created to evaluate a single-cells' response to experiencing a series of iterative deformations and use their velocities in these deformation regions to discriminate metastatic cancer at the single-cell level [66]. These results exhibit the viability of using mechanical deformation in microfluidics as a trusted method of evaluating the biomechanical properties of cells. In this paper, we introduce new methods of evaluating the biophysical properties of cells. Chapter 2 will focus on the biomechanical properties of cells by showing how multiple deformation regions can be used to better distinguish normal and cancer cells. In chapter 3, we enhance the previous single-channel/single-deformation design with one device that has higher-resolution velocity measurements and another device with improved

throughput using parallel deformation channels. Chapter 4 will include a conclusion along with the future outlook of this body of work.

References:

1. *Cancer*. Available from: http://www.who.int/mediacentre/factsheets/fs297/en/.
2. *Metastatic Cancer*. Available from: https://www.cancer.gov/types/metastatic-cancer.
3. Chaffer, C.L. and R.A. Weinberg, *A perspective on cancer cell metastasis.* Science, 2011. **331**(6024): p. 1559-1564.
4. Siegel, R., et al., *Cancer statistics, 2014.* CA: a cancer journal for clinicians, 2014. **64**(1): p. 9-29.
5. Siegel, R.L., K.D. Miller, and A. Jemal, *Cancer statistics, 2016.* CA: a cancer journal for clinicians, 2016. **66**(1): p. 7-30.
6. Corbin, E.A., et al., *Biophysical properties of human breast cancer cells measured using silicon MEMS resonators and atomic force microscopy.* Lab on a Chip, 2015. **15**(3): p. 839-847.
7. Zheng, Y., et al., *Recent advances in microfluidic techniques for single-cell biophysical characterization.* Lab on a Chip, 2013. **13**(13): p. 2464-2483.
8. Ujihara, Y., M. Nakamura, and S. Wada, *A mechanical cell model and its application to cellular biomechanics*, in *Biomedical Engineering-From Theory to Applications*. 2011, InTech.
9. Elson, E.L., *Cellular mechanics as an indicator of cytoskeletal structure and function.* Annual review of biophysics and biophysical chemistry, 1988. **17**(1): p. 397-430.
10. *Microtubules and Filaments.* Available from: https://www.nature.com/scitable/topicpage/microtubules-and-filaments-14052932.
11. Satcher, R. and C.F. Dewey, *Theoretical estimates of mechanical properties of the endothelial cell cytoskeleton.* Biophysical journal, 1996. **71**(1): p. 109-118.
12. *Cytoskeleton.* Available from: https://sites.google.com/site/cellworldhollllaaaa/home/cytoskeleton.
13. Nagayama, K. and T. Matsumoto. *EFFECTS OF ACTIN FILAMENTS AND MICROTUBULES ON QUASI-IN SITU TENSILE PROPERTIES AND INTRACELLULAR FORCE BALANCE OF CULTURED AORTIC SMOOTH MUSCLE CELLS (1A2 Micro & Nano Biomechanics II)*. in *The Proceedings of the Asian Pacific Conference on Biomechanics: emerging science and technology in biomechanics 2007.3*. 2007. The Japan Society of Mechanical Engineers.
14. Yu, C.-H., et al. *Morpho: A self-deformable modular robot inspired by cellular structure*. in *Intelligent Robots and Systems, 2008. IROS 2008. IEEE/RSJ International Conference on*. 2008. IEEE.
15. Ingber, D.E., *Tensegrity and Complex Systems Biology.*
16. Ingber, D.E., *Cellular tensegrity: defining new rules of biological design that govern the cytoskeleton.* Journal of Cell Science, 1993. **104**(3): p. 613-627.
17. Ingber, D.E., *Tensegrity I. Cell structure and hierarchical systems biology.* Journal of cell science, 2003. **116**(7): p. 1157-1173.
18. Ingber, D.E., *Tensegrity II. How structural networks influence cellular information processing networks.* Journal of cell science, 2003. **116**(8): p. 1397-1408.
19. Stamenović, D., et al., *Experimental tests of the cellular tensegrity hypothesis.* Biorheology, 2003. **40**(1, 2, 3): p. 221-225.

20. Wang, N., et al., *Cell prestress. I. Stiffness and prestress are closely associated in adherent contractile cells.* American Journal of Physiology-Cell Physiology, 2002. **282**(3): p. C606-C616.
21. *Cells, Biological.* Available from: http://tensegritywiki.com/Cells%2CBiological.
22. Hur, S.C., et al., *Deformability-based cell classification and enrichment using inertial microfluidics.* Lab on a Chip, 2011. **11**(5): p. 912-920.
23. Guck, J., et al., *Optical deformability as an inherent cell marker for testing malignant transformation and metastatic competence.* Biophysical journal, 2005. **88**(5): p. 3689-3698.
24. Hou, H.W., et al., *Deformability study of breast cancer cells using microfluidics.* Biomedical microdevices, 2009. **11**(3): p. 557-564.
25. Lincoln, B., et al., *Reconfigurable microfluidic integration of a dual-beam laser trap with biomedical applications.* Biomedical microdevices, 2007. **9**(5): p. 703-710.
26. Lincoln, B., et al., *Deformability-based flow cytometry.* Cytometry Part A, 2004. **59**(2): p. 203-209.
27. Swaminathan, V., et al., *Mechanical stiffness grades metastatic potential in patient tumor cells and in cancer cell lines.* Cancer research, 2011. **71**(15): p. 5075-5080.
28. Byun, S., et al., *Characterizing deformability and surface friction of cancer cells.* Proceedings of the National Academy of Sciences, 2013. **110**(19): p. 7580-7585.
29. Suresh, S., *Biomechanics and biophysics of cancer cells.* Acta Materialia, 2007. **55**(12): p. 3989-4014.
30. Hochmuth, R.M., *Micropipette aspiration of living cells.* Journal of biomechanics, 2000. **33**(1): p. 15-22.
31. Hoffman, R.M., *Imaging the role of the tumor microenvironment in tumor progression and metastasis.* Cancer Cell & Microenvironment, 2016. **3**(2).
32. Lee, G.Y. and C.T. Lim, *Biomechanics approaches to studying human diseases.* Trends in biotechnology, 2007. **25**(3): p. 111-118.
33. Cross, S.E., et al., *Nanomechanical analysis of cells from cancer patients.* Nature nanotechnology, 2007. **2**(12): p. 780-783.
34. Lekka, M., et al., *Elasticity of normal and cancerous human bladder cells studied by scanning force microscopy.* European Biophysics Journal, 1999. **28**(4): p. 312-316.
35. Rosenbluth, M.J., W.A. Lam, and D.A. Fletcher, *Force microscopy of nonadherent cells: a comparison of leukemia cell deformability.* Biophysical journal, 2006. **90**(8): p. 2994-3003.
36. Wang, N. and D.E. Ingber, *Probing transmembrane mechanical coupling and cytomechanics using magnetic twisting cytometry.* Biochemistry and Cell Biology, 1995. **73**(7-8): p. 327-335.
37. Suresh, S., et al., *Reprint of: connections between single-cell biomechanics and human disease states: gastrointestinal cancer and malaria.* Acta biomaterialia, 2015. **23**: p. S3-S15.
38. Darling, E.M. and D. Di Carlo, *High-throughput assessment of cellular mechanical properties.* Annual review of biomedical engineering, 2015. **17**: p. 35-62.
39. Xu, W., et al., *Cell stiffness is a biomarker of the metastatic potential of ovarian cancer cells.* PloS one, 2012. **7**(10): p. e46609.

40. Gossett, D.R., et al., *Hydrodynamic stretching of single cells for large population mechanical phenotyping.* Proceedings of the National Academy of Sciences, 2012. **109**(20): p. 7630-7635.
41. Yoshino, T., et al., *Evaluation of cancer cell deformability by microcavity array.* Analytical biochemistry, 2017. **520**: p. 16-21.
42. Irimajiri, A., et al., *Dielectric Modeling of Biological Cells: Models and Algorithm (Commemoration Issue Dedicated to Professor Tetsuya HANAI On the Occasion of His Retirement).* 1991.
43. Salimi, E., et al., *Dielectric model for Chinese hamster ovary cells obtained by dielectrophoresis cytometry.* Biomicrofluidics, 2016. **10**(1): p. 014111.
44. Morgan, H., et al., *Single cell dielectric spectroscopy.* Journal of Physics D: Applied Physics, 2006. **40**(1): p. 61.
45. Heileman, K., J. Daoud, and M. Tabrizian, *Dielectric spectroscopy as a viable biosensing tool for cell and tissue characterization and analysis.* Biosensors and Bioelectronics, 2013. **49**: p. 348-359.
46. Ducote M, V.B., Hogquist S, Riggs B, Saksena J, *Electrochemical Impedance Spectroscopy (EIS) as a Tool for Pathogen Detection.* Journal of Biosensors and Bioelectronics, 2016. **7**(224).
47. Wegener, J., C.R. Keese, and I. Giaever, *Electric cell–substrate impedance sensing (ECIS) as a noninvasive means to monitor the kinetics of cell spreading to artificial surfaces.* Experimental cell research, 2000. **259**(1): p. 158-166.
48. Cheung, K., S. Gawad, and P. Renaud, *Impedance spectroscopy flow cytometry: on-chip label-free cell differentiation.* Cytometry Part A, 2005. **65**(2): p. 124-132.
49. Han, A., L. Yang, and A.B. Frazier, *Quantification of the heterogeneity in breast cancer cell lines using whole-cell impedance spectroscopy.* Clinical cancer research, 2007. **13**(1): p. 139-143.
50. Wei, Y., et al., *Embedded silver PDMS electrodes for single cell electrical impedance spectroscopy.* Journal of Micromechanics and Microengineering, 2016. **26**(9): p. 095006.
51. Heidmann, I., et al., *Impedance Flow Cytometry: A Novel Technique in Pollen Analysis.* PloS one, 2016. **11**(11): p. e0165531.
52. David, F., et al., *Viability and membrane potential analysis of Bacillus megaterium cells by impedance flow cytometry.* Biotechnology and bioengineering, 2012. **109**(2): p. 483-492.
53. Asphahani, F., et al., *Single-cell bioelectrical impedance platform for monitoring cellular response to drug treatment.* Physical biology, 2011. **8**(1): p. 015006.
54. Liu, Q., et al., *Impedance studies of bio-behavior and chemosensitivity of cancer cells by micro-electrode arrays.* Biosensors and Bioelectronics, 2009. **24**(5): p. 1305-1310.
55. Schwarzenberger, T., et al., *Impedance sensor technology for cell-based assays in the framework of a high-content screening system.* Physiological measurement, 2011. **32**(7): p. 977.
56. Yu, J., et al., *Nanoporous membrane-based cell chip for the study of anti-cancer drug effect of retinoic acid with impedance spectroscopy.* Talanta, 2009. **80**(1): p. 189-194.
57. Adamo, A., et al., *Microfluidics-based assessment of cell deformability.* Analytical chemistry, 2012. **84**(15): p. 6438-6443.
58. Cheung, K.C., et al., *Microfluidic impedance-based flow cytometry.* Cytometry Part A, 2010. **77**(7): p. 648-666.

59. Ghenim, L., et al., *Monitoring impedance changes associated with motility and mitosis of a single cell.* Lab on a Chip, 2010. **10**(19): p. 2546-2550.
60. Wang, L., et al., *Real-time, label-free monitoring of the cell cycle with a cellular impedance sensing chip.* Biosensors and Bioelectronics, 2010. **25**(5): p. 990-995.
61. *The cell cycle, mitosis and meiosis.* Available from: http://www2.le.ac.uk/projects/vgec/schoolscolleges/topics/cellcycle-mitosis-meiosis.
62. Jang, L.-S., et al., *Design and fabrication of microfluidic devices integrated with an open-ended MEMS probe for single-cell impedance measurement.* Microfluidics and Nanofluidics, 2010. **8**(4): p. 509-519.
63. Malleo, D., et al., *Continuous differential impedance spectroscopy of single cells.* Microfluidics and nanofluidics, 2010. **9**(2-3): p. 191-198.
64. Nikkhah, M., *Identification of Cell Biomechanical Signatures Using Three Dimensional Isotropic Microstructures*. 2010.
65. Babahosseini, H., et al., *The impact of sphingosine kinase inhibitor-loaded nanoparticles on bioelectrical and biomechanical properties of cancer cells.* Lab on a Chip, 2016. **16**(1): p. 188-198.
66. Babahosseini, H., J.S. Strobl, and M. Agah, *Microfluidic iterative mechanical characteristics (iMECH) analyzer for single-cell metastatic identification.* Analytical Methods, 2017. **9**(5): p. 847-855.

2. Single-Cell Mechanical Characteristics Analyzed by Multi-Constriction Microfluidic Channels

This chapter is produced from [41] with permission from the American Chemical Society.

Ren, X., Ghassemi, P., Babahosseini, H., Strobl, J. S., & Agah, M., Single-Cell Mechanical Characteristics Analyzed by Multiconstriction Microfluidic Channels. ACS Sensors, 2017. ***2****(2), p. 290-299.*

My contributions towards this body of work included device fabrication, sample preparation, experimentation and data collection. Device fabrication included using our designed and fabricated SU-8 mold to create PDMS microfluidic channels using soft lithography techniques, which were then bonded onto glass slides using plasma-activated bonding. Sample preparation involved creating a single-cell suspension by trypsinization of adherent cell culture and subsequent suspension in respective cell culture medium. I was involved in experimental setup and execution by collecting high-speed videos of cell transition in the parallel microfluidic channel. To collect velocities of the cell's transition in the constriction channels, post-processing of the high-speed videos was done. In addition, I assisted with the writing of the manuscript.

2.1 Introduction:

Studies of the mechanical characteristics of single cells have been previously used in cancer research [1,2]. Different stages of cancer cells have significant mechanical differences due to the stiffness of their cell membrane [3]. Other well-developed methods and techniques based on cell membrane properties, the epithelial cell adhesion molecule (EpCAM) and fluorescence detection for the sorting of cancer cells require specific equipment, such as atomic force microscopy [3,4],

costly antibody reagents [5,6] and flow cytometry setups [7-10]. Microfluidic chips bring new technologies and methods to both cancer cells analysis and circulating tumor cell (CTC) detection and sorting [11]. Size-based microfluidic channels for CTC cancer cell separation are broadly used in CTC studies which sense the different diameters of cancer cells, white blood cells and red blood cells [12-17]. In order to analyze and sort different cancer cells with similar sizes, investigators have chosen to use constriction channels and study the dynamics of cells, usually accompanied by other methods sensitive to both biomechanical and bioelectrical properties to enable identification [18-22].

Characterization of the mechanical properties of cancer cells using a microfluidic device with constriction channels has been proven to be an accurate method to differentiate different cell lines [23-26]. Metastatic cancer cells have softer cell membranes, as well as deformation ability in microfluidic constriction channels. On the other hand, normal cells have a cytoskeleton with higher mechanical strength, including but not limited to actin filaments, intermediate filaments, and microtubules [27, 28]. Therefore, the deformation time of cancer cells and normal cells has been shown to differ due to their mechanical properties. Many studies have focused on the entry time and transit time of cells in a constriction channel, and analysis has defined criteria typifying specific cell lines [29]. By plotting the dynamic parameters of the single cells in constriction channel, different cell lines, including breast cancer cells [3, 18, 23], lung cancer cells [19, 30, 31], kidney tumor cells [32], and cervical cancer cell lines [33, 34], can be separated into groups in order to achieve cell characterization [35]. However, using a single constriction channel or adjustable constriction channels have limited capabilities to distinguish between cancer cells and normal cells. When differentiating various cell lines, scientists studying characterization of cancer cells have added an additional bioelectrical measurement along with the single constriction

channel [2, 20]. At the same time, improvements in the methods used to induce cells' deformation using not only constriction channels, but also lateral displacement array or pillar array [17,36] in a microfluidic chamber [13, 14] have enhanced the resolution of characterizing cells.

This manuscript reports a multi-constriction multi-channel microfluidic device for analyzing velocity profiles of single-cells which provides greater single-cell resolution of normal and cancer cells than that afforded by a single constriction channel studies. Smartphone video-microscopy was used to capture the dynamic motions of cells as each passed through the series of constriction channels. The result was a distinct velocity profile at each stage of deformation in the multiple constriction channels. Compared to single-constriction channels, multi-constriction channels divide the cell deformation into multiple stages, which effectively reveals the deformation process of each cell with higher resolution, and hence a new and simple way to observe the variations in individual cells' velocity profiles. The series of relaxation regions separating the constriction channels causes cells to experience multiple relaxations where cell membrane/shape recovery takes place. The length of relaxation regions are kept as 50 μm constantly, so that the results can focus on the effects of the constriction, the relaxation count and constriction length. The microfluidic channels device was designed with three different configurations to compare the ability to differentiate two different cell lines in each channel. We also compared the effect of adding one or multiple relaxation regions in the constriction channel. The velocity profiles analyses were focused on comparing the initial velocity change due to the deformation at the entrance of each channel and the exiting velocity at the last segment of the channel, where the cells have experienced sufficient deformations. The multiple deformation procedure increases the ability of deformation and recovery of the cells. Based on our experimental results, the ability to differentiate between cancer cells and normal cells in a multi-constriction

channel is higher than that achieved with either a single constriction channel or two constriction channels with only one relaxation region. After establishing criteria to examine the difference between initial velocities and final velocities, we successfully differentiated ~94.3% of the cancer cells from normal cells. Then, four testing samples were used to verify our criteria. The results indicated that the selected criteria for the multi-constriction channels have an accuracy around 95% to tell the difference between cancer cells and normal cells.

2.2 Materials and Methods

Cell culture and sample preparation

We prepared the highly metastatic breast cancer cells MDA-MB-231 and benign breast epithelial cells MCF-10A to represent normal cells with the same concentration of ~50,000 cells/mL. Both MDA-MB-231 and MCF-10A cells were provided by the Tissue Culture Shared Resources of the Lombardi Comprehensive Cancer Center, Georgetown University in Washington, DC. MDA-MB-231 cells were grown in F12:DMEM (Lonza, Basel, Switzerland) with 10% fetal bovine serum (FBS), 4 mM glutamine and penicillin-streptomycin (100 units per mL). MCF-10A cells were grown in F12:DMEM with penicillin-streptomycin (100 units per mL), 2.5 mM L-glutamine, 20 ng/mL epidermal growth factor (EGF), 0.1 μg/mL cholera toxin, 10 μg/mL insulin, 0.5 μg/mL hydrocortisone, and 5% horse serum. The cells were grown in T-25 cm2 culture flasks at 37°C in a 5% CO2 in air atmosphere until cells were ready for subculture.

The morphology of the cells was observed before trypsinization (Figure 2.1). The cells were then detached from the flask with Trypsin-EDTA solution (Trypsin-EDTA solution 10X, , Sigma); The MDA-MB-231 cells were trypsinized at 37°C for 2 min and MCF-10A cells were trypsinized at 37°C for 15 min. Before every experiment, the viability of the cells was observed under a microscope using trypan blue (Trypan blue solution (0.4%), Lot. 42K2360, Sigma) 37. Both trypan

blue and culture medium were warmed to 37°C in a water bath before usage. The viability of the cells was 100%, as determined by the count using a hemocytometer.

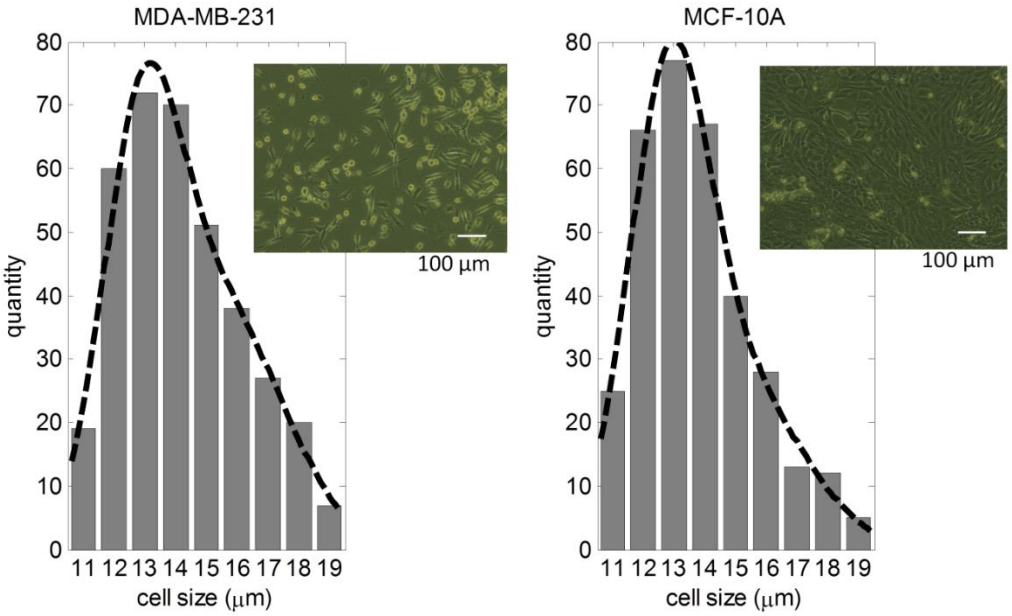

Figure 2.1: MDA-MB-231, MCF-10A cell size distribution; cell image before trypsinization.

Microfluidic channel fabrication

The multi-constriction channels devices were fabricated on a silicon wafer with two layers of SU-8 (SU-8 3005 and SU-8 3025, MicroChem, Newton, MA) photolithography and polydimethylsiloxane (PDMS) soft-lithography, followed by PDMS and glass bonding after plasma treatment. Three different configurations of channels were connected to a main delivery channel, as shown in the channel configurations in Figure 2.2. All the constriction channels had a cross-section of 8 μm by 8 μm. The first channel contains only one constriction channel with a length of 250 μm; the second channel contains two constriction channels with lengths of 125 μm each, and a relaxation section with a length of 50 μm; the third channel contains five constriction channels with a length of 50 μm each, and relaxation sections of 50 μm between every constriction channel.

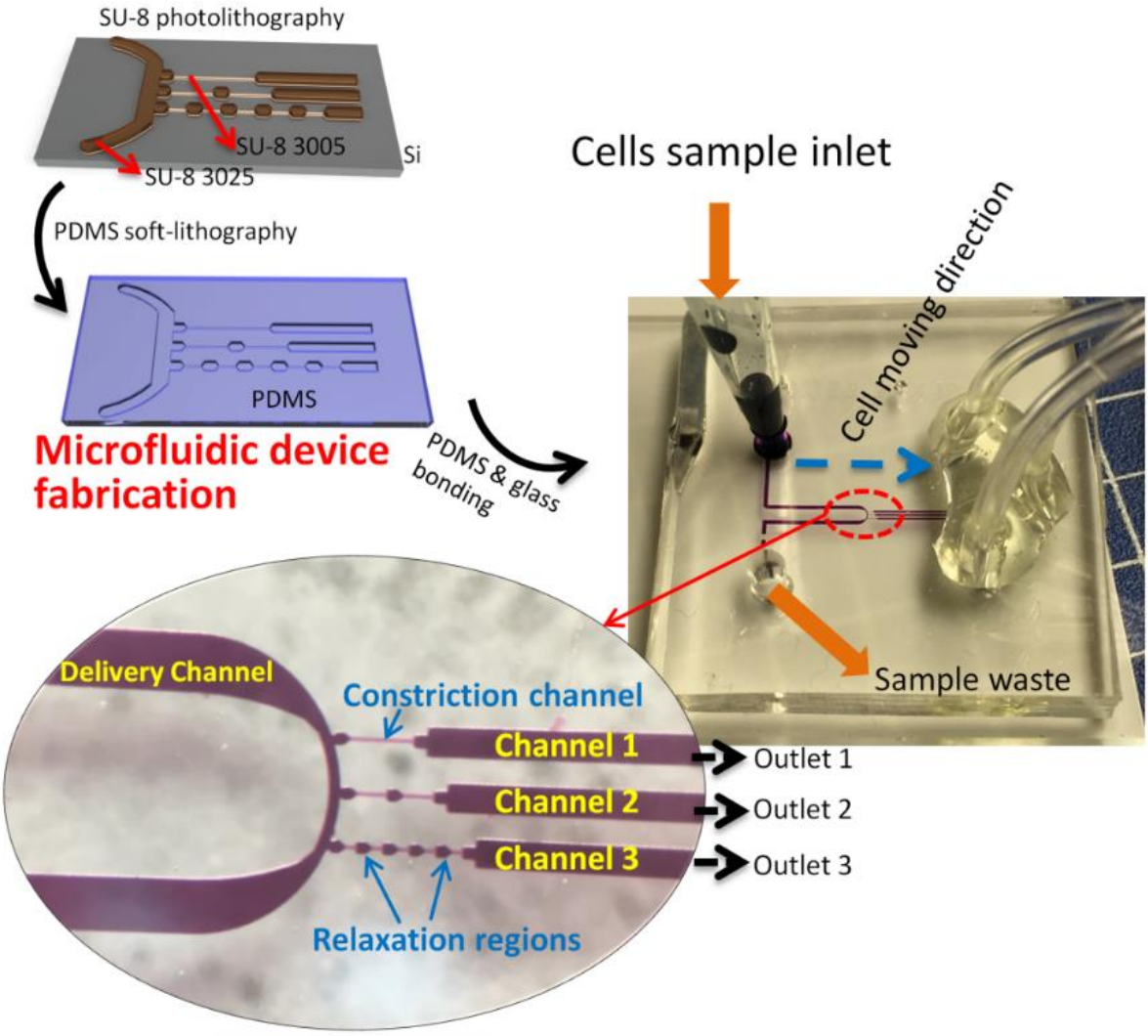

Figure 2.2: Microfluidic device fabrication processes.

The SU-8 mold consists of two layers with 8 μm of SU-8 3005 and ~25 μm of SU-8 3025, as illustrated in Figure 2.2. Tridecafluoro-1,1,2,2-tetrahydrooctyl-1-trichlorosilane (TFOCS, Fisher Scientific) was coated on the surface of the molds for the easy release of PDMS. After the mold was prepared, standard PDMS (SYLGARD® 184, Dow Corning, Midland, MI) replica molding was conducted to fabricate the microchannels. The PDMS channels were then bonded to a glass slide after air plasma treatment using plasma cleaner (Harrick Plasma, model PDC-001, Ithaca, NY).

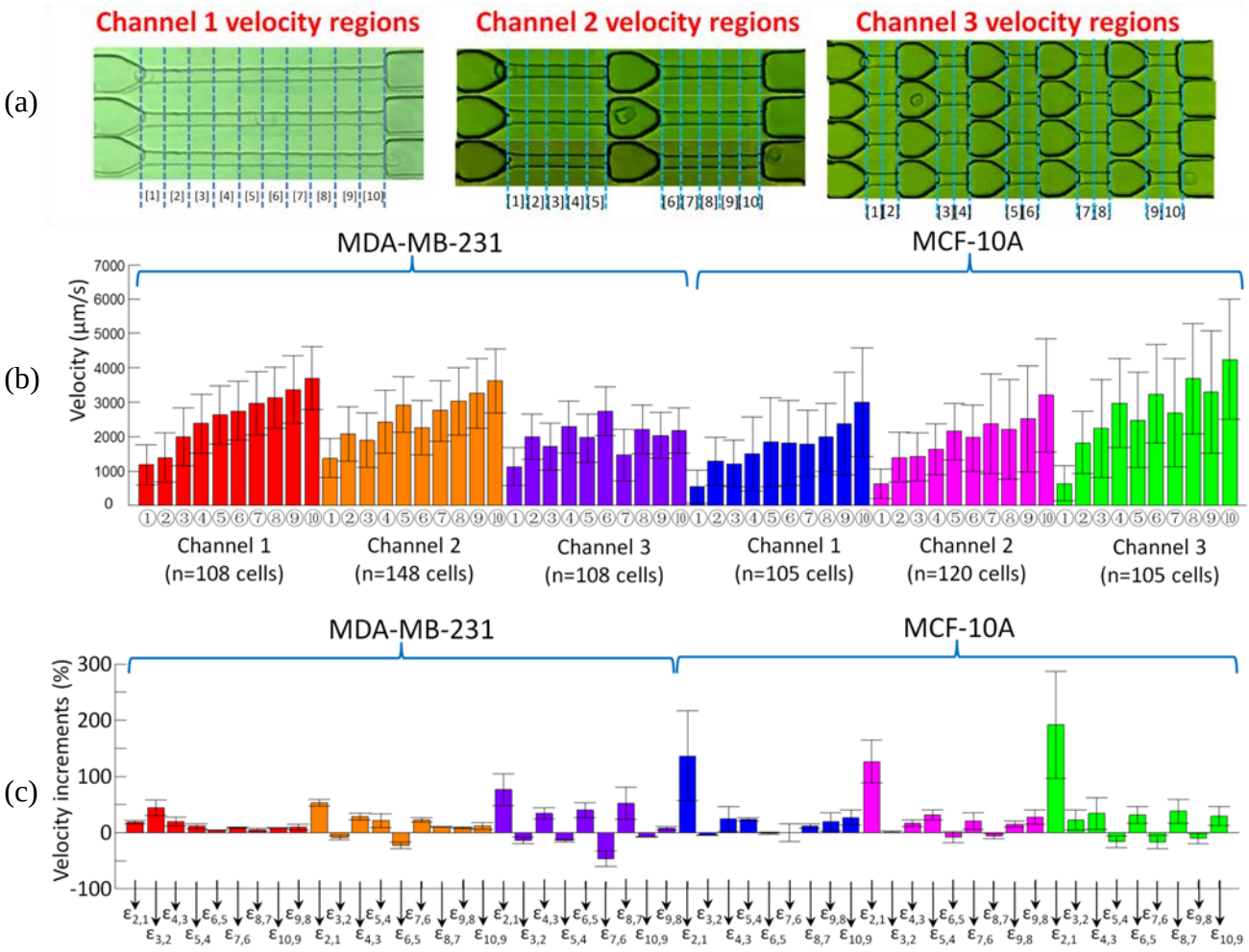

Figure 2.3: (a) Defining the velocity regions in three channel configurations using segment ①~⑩; The (b) velocity and (c) velocity increments of MDA-MB-231 cells and MCF-10A cells in three different microfluidic channels.

2.3 Experimental

Experimental setup

The microfluidic device was mounted on an inverted microscope (Zeiss Axio Observer, LSM-510, Thornwood, NY) with a lens magnification of 20×. One side of the delivery channel was connected to a reservoir with a cell sample. Three outlets were connected together to a syringe pump to create the same negative pressure. The cell delivery was initiated by applying a one-time negative pressure by another vacuum pump. The cell delivery was maintained by the pressure

difference between the cell sample reservoir and the opening of the other side of the delivery channel. This channel dimension is good for cell sizes from 11 μm to 19 μm. Normal cells (MCF-10A) with 25 μm or larger will completely clog the microchannel.

Instead of a high speed camera, a smartphone's slow motion function was applied to record videos of cell movement with a frame rate of 240 frames per second. The video can be analyzed to extract information about the motion of each cell traveling through the constriction channels. As shown in Figure 2.2, the single constriction channel was referred as channel 1; the middle channel with one relaxation at 125 μm was referred as channel 2; and the five-constriction and four relaxation channel was referred as channel 3.

Data collection

The data of the movement of the cells in the three different channels were collected from the smartphone videos. For analysis, only the constriction channels were considered, where all three channels have the same total length of 250 μm in constrictions. The velocity distribution for every 25 μm was plotted in Matlab. As shown in Figure 2.3, the velocity at each segment was represented as ① to ⑩. The velocities in segments ① to ⑩ were recorded as V1, V2, V3, … , V10, respectively. Next, the velocity increment between every 25 μm was calculated. The velocity increments between two segments are defined as: $\varepsilon_{m,n} = \frac{V_m - V_n}{V_n}$, where m = 1,2,3,…,8,9, 10, and n = 1,2,3,…,8,9, 10, representing ten segments in constriction channel.

2.4 Results

Velocity of the cells

The velocity and the increments of velocity between every 25 μm of both MDA-MB-231 and MCF-10A in three channels are demonstrated in Figure 2.3. Each cell line in every channel is represented by a color, and the same color will be used in the single cell analysis.

The initial entry velocity of MDA-MB-231 cells was similar regardless of the number of relaxation regions. This can be seen in Figure 2.3(b) by comparing the heights of the red bar ①, orange bar ① and purple bar ① into channel 1, channel 2, and channel 3 as shown in the channel configurations in Figure 2.3(b), respectively. Similarly, the initial entry velocity of MCF-10A cells was independent of the number of relaxation regions as can be seen by comparing the heights of blue bar ①, pink bar ① and green bar ①. These results serve to validate the measurement system because the aperture to each channel type (channel 1, channel 2, and channel 3) is identical. Due to the same dimension of the entrance of constriction channels, the same cell line had a similar entry velocity in channel 1~3.

As seen in Figure 2.3(b), the initial entry velocity measurement of MDA-MB-231 cells entered segment ① of each channel twice as fast as MCF-10A cells. Also shown in Figure 2.3(b), from the initial entry velocity of the MDA-MB-231 cells in channel 1, 2 and 3 (red bar ①, orange bar ①, and purple bar ①, respectively), the average velocity of MDA-MB-231 cells was measured as ~1.2×10^3 μm/s, with a standard deviation of ~0.6×10^3 μm/s. Also from Figure 2.3(b), from the initial entry velocity of the MCF-10A cells in channel 1, 2 and 3 (blue bar ①, pink bar ①, and green bar ①, respectively), the average velocity of MCF-10A cells was measured as 594.0 μm/s, with a standard deviation of 473.0 μm/s.

We assume the initial entry velocity

$$\overline{V_{CA}} = k \cdot \overline{V_{NR}}$$

where k represent how much times the velocity of cancer cells is compared to normal cells. Using $\alpha = 0.05$, the t_k in t-test is 1.647; therefore, k=1.92. This means that the probability of the initial velocity of cancer cells is 1.92 times to normal cells is larger than 95%. If $k = 2$, which means $\overline{V_{CA}} > 2 \cdot \overline{V_{NR}}$, the possibility p = 79.87%. Similarly, if $\overline{V_{CA}} > 1.86 \cdot \overline{V_{NR}}$, the possibility p = 99%.

Table 2.1: Velocity difference calculated by the velocity profiles in Figure 2.3.

	MDA-MB-231			MCF-10A		
channel	1	2	3	1	2	3
$\varepsilon_{2,1}$	1.36	1.26	1.91	0.18	0.53	0.76
channel		2			2	
$\varepsilon_{6,5}$		-0.23			-0.08	

It is well-recognized that metastatic cancer cells are softer than normal cells [2, 25, 26] and this has been correlated with faster deformation and transit times in constriction channels [3, 33, 31, 38]. Here we have improved the resolution of such studies by analyzing velocity profiles. The initial velocity incremental difference between MDA-MB-231 cells and MCF-10A cells was further analyzed as illustrated by Figure 2.3c. $\varepsilon_{2,1}$ is defined by the equation: $\varepsilon_{2,1} = (\mathrm{V}_2 - \mathrm{V}_1)/\mathrm{V}_1$. As calculated velocity difference (Table 2.1) from Figure 2.3c, the average $\varepsilon_{2,1}$ of the MCF-10A cells in channel 1 (blue), channel 2 (pink), and channel 3 (green) is 1.36, 1.26, 1.91, respectively (Table 2.1). This shows that after 25 μm of deformation, MCF-10A cells reach a much higher V2 compared to the initial entry velocity V1. However, the $\varepsilon_{2,1}$ of MDA-MB-231 cells was calculated to be 0.18, 0.53 and 0.76, respectively for channels 1, 2, and 3; these data indicated a slight decrease in the velocity of the MDA-MB-231 cells after their initial entry into the channel. This at first seems inconsistent with the "softer" biomechanical nature of the cancer cells, and we investigated this in greater depth.

The average velocity profiles can indicate the heterogeneity of the population of a cell-line. However, we need to analyze the detailed velocity differences in each segment to find the different mechanical characteristics. Channel 2 has one relaxation region between segment ⑤ and ⑥ (as illustrated in the "channel 2" in Figure 2.3(c)). The velocity has a drop for both MDA-MB-231

cells and MCF-10A cells at V6 compared to V5, as shown in segment ⑥ of the orange and pink in Figure 2.3(b). $\varepsilon_{6,5}$ is defined by the equation: $\varepsilon_{6,5} = (V_6 - V_5)/V_5$. As calculated velocity difference (Table 2.1) from Figure 2.3(c), the average $\varepsilon_{6,5}$ of the MDA-MB-231 cells and the MCF-10A cells in channel 2 (orange and pink), is -0.23 and -0.08, respectively. This indicated that the velocity of MDA-MB-231 cells had been reduced more than MCF-10A cells. In another word, MCF-10A cells inherited a higher more exiting velocity after the relaxation region between segment ⑤ and ⑥. Channel 3 contains five constriction channels, each 50 μm in length, separated by relaxation sections of 50 μm between every constriction channel. Cells deformed at the entrance of the first constriction channel (defined as segment ① in the "channel 3" in Figure 2.3(b)) and exited at the last segment of the final constriction channel (defined as segment ⑩ in the "channel 3" in Figure 2.3(b)), where the cells have experienced sequential deformations. Cancer cells recovered back to a round cell shape quicker than normal cells in each relaxation segment and we defined this as "deformation performance". Therefore, the cancer cells showed deformation performance at the entrance to each constriction channel, which resulted in a decreasing velocity.

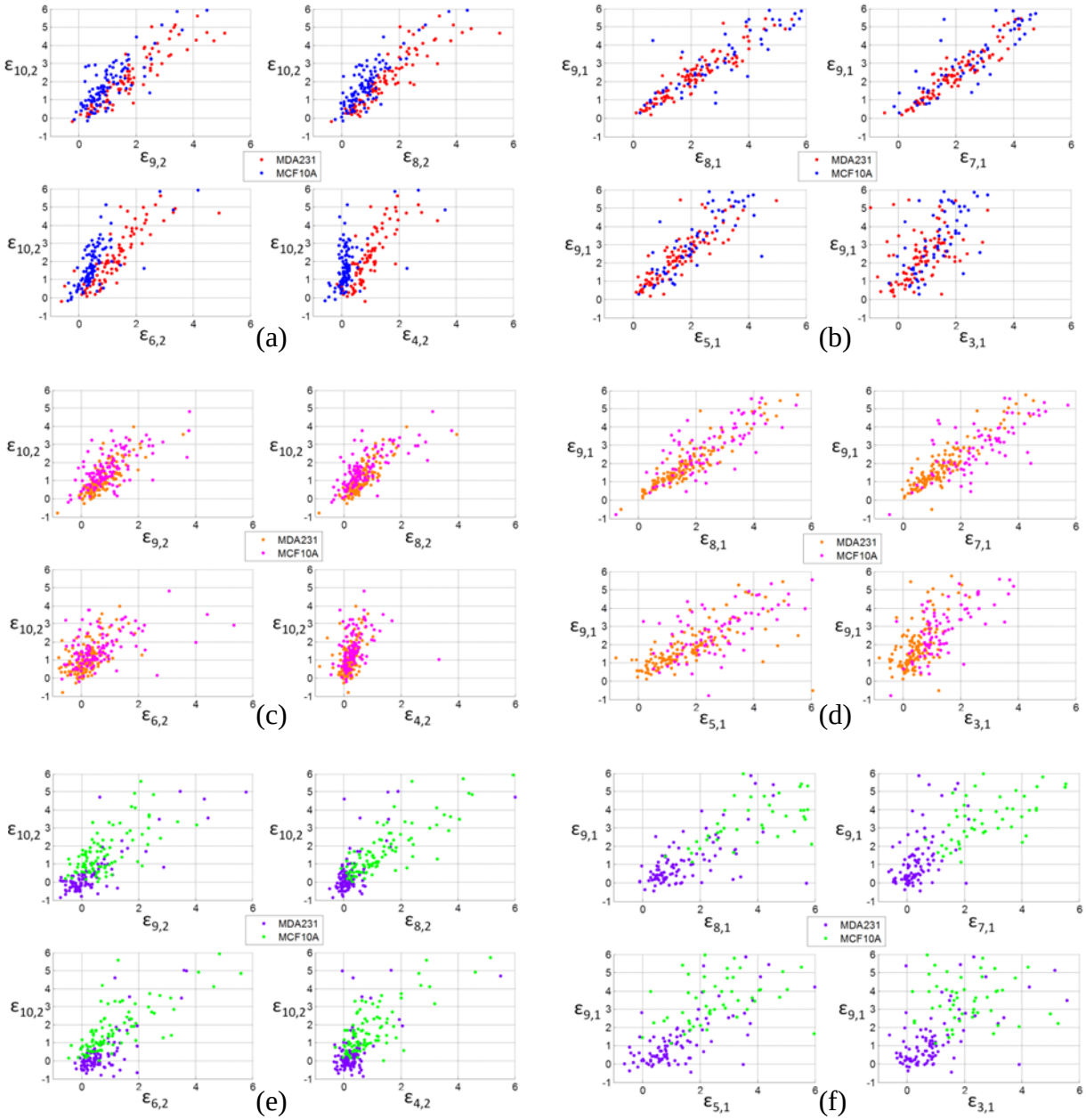

Figure 2.4: Scatter plot of MDA-MB-231 cells and MCF-10A cells velocity increments of comparing $\varepsilon_{10,2}$ to $\varepsilon_{9,2}$, $\varepsilon_{8,2}$, $\varepsilon_{6,2}$, and $\varepsilon_{4,2}$ in channel 1 (a), channel 2 (c), and channel 3 (e); and comparing $\varepsilon_{9,1}$ to $\varepsilon_{8,1}$, $\varepsilon_{7,1}$, $\varepsilon_{5,1}$, and $\varepsilon_{3,1}$ in channel 1 (b), channel 2 (d), and channel 3 (f).

As shown in Figure 2.3(a), the initial velocities (segment ①, 0~25 μm traveling distance in constriction channel) of MDA-MB-231 cells were ~1100 μm/s (purple bar ①), and exiting velocities (segment ⑩, 215~250 μm traveling distance in constriction channel) were ~2200 μm/s

(purple bar ⑩). In contrast, normal cells deformed slower initially, but reached a relatively higher velocity after two or three deformations. Normal cells stay in a rod-like shape without fully recovering back to an original spherical shape. The initial velocities of MCF-10A cells were ~600 μm/s (green bar ①), and exiting velocities were ~4100 μm/s (green bar ⑩). The geometry shapes of normal cells were almost fixed when the normal cells entered the fourth and fifth constriction channels. The entrance time of cancer cells into the fourth and fifth channel was longer than the normal cells.

Single cell velocity analysis

In order to illustrate how well MDA-MB-231 and MCF-10A cells can be differentiated at the single cell level, Figure 2.4 presents the scatter plots of single cell velocity data in each channel using the same color legend as in Figure 2.3. Each dot represents the data of one cell.

The scatter plot of the MDA-MB-231 and MCF-10A cells' velocity differences in channel 1, 2, and 3 calculated at different regions within each channel are shown in Figure 2.4. The data from Channel 1 is the focus in Figure 2.4(a) and 2.4(b). Here it can been seen when comparing $\varepsilon_{10,2}$ and $\varepsilon_{9,1}$, (the ending velocity (V9 and V10), respectively) and the entry velocities (V1 and V2), the MDA-MB-231 (red dots) and MCF-10A cells (blue dots) had major overlaps in channel 1. The velocity profiling using the channel 1 configuration cannot distinguish between the cancer and normal cells at the single-cell level. About 95% of the cancer cells will be recognized as normal cells by the criterion $\varepsilon_{10,2} < 0$. Almost no cells have $\varepsilon_{10,2} > 0$, which means both MDA-MB-231 cells and MCF-10A cells have completely deformed and accelerated during passage through the single, 250 μm constriction channel. Compared to $\varepsilon_{8,2}$, and $\varepsilon_{6,2}$ in Figure 2.4(a), the criterion $\varepsilon_{4,2}$ showed a better segregation of red and blue dots into two separate regions. V1 and V2 represent the beginning of the constriction channel, where cells begin to deform. MDA-MB-231 and MCF-10A

cells showed a different deformation performance during the first 100 μm of the channel 1. MDA-MB-231 cells took a shorter time to reach a higher velocity than MCF-10A cells at V4. Therefore, the $\varepsilon_{4,2}$ of MDA-MB-231 cells had a higher value than MCF-10A cells in Figure 2.4(a). This phenomenon supports atomic force microscopy (AFM) data showing that MCF-10A cells were stiffer than MDA-MB-231 cells [2, 3, 38], which might account for inability of MCF10A cells to reach higher velocities in a continuous constriction channel of 250 μm.

Channel 2: As shown in Figure 2.4(c) and 2.4(d), the relaxation region between velocity segments ⑤ and ⑥ of the constriction channel 2 separated the channel into two 125 μm channels. The scatter plot of MDA-MB-231 cells (orange dots) and MCF-10A cells (pink dots) had major overlap at both in $\varepsilon_{10,2}$ and $\varepsilon_{9,1}$ regions, as well as in different velocity segments, such as $\varepsilon_{8,2}$, $\varepsilon_{7,1}$, $\varepsilon_{5,1}$ and $\varepsilon_{3,1}$. Because the complete deformation of MDA-MB-231 and MCF-10A cells was achieved by around the 100 μm mark within channel 2, the velocity differences were similar for both of these cell types within each velocity segment. The scatter plot in Figure 2.4(c) and 2.4(d) indicated that the channel 2 configuration was not useful in differentiating MDA-MB-231 and MCF-10A cells.

In channel 3, the short relaxation and constriction allowed the cells to continue experiencing a secondary deformation after the first relaxation. As shown in Figure 2.4(e) and 2.4(f), all of the MCF-10A cells (purple dots) had $\varepsilon_{10,2}>0$, and the majority of MDA-MB-231 cells (green dots) fell into $\varepsilon_{10,2}<0$. By further consideration of $\varepsilon_{7,1}$, more cancer cell dots fell into the region where $\varepsilon_{7,1}<2$. V7 was the velocity in the fourth constriction region in channel 3. Therefore, based on the scatter plots of MDA-MB-231 and MCF-10A cells, it is possible using the channel 3 configuration to accurately identify individual single cell from either the MDA-MB-231 or MCF-10A cell line. The $\varepsilon_{4,2}$ in Figure 2.4(a) had a separation between MDA-MB-231 and MCF-10A

cells. In channel 1, using criterion of $\varepsilon_{4,2}>0.5*\varepsilon_{2,1}$, the false negative (cancer cells observed as normal cells) rate is 7.4%, and the false positive (normal cells observed as cancer cells) rate is 19%. Using criteria of $\varepsilon_{4,2}> 0.5*\varepsilon_{2,1}$ and $\varepsilon_{4,2}>0.3$, the false negative rate is 7.4%, and the false positive rate is 19%, which means that the $\varepsilon_{4,2}$ does not further improve the differentiation rate. If we include more criteria, such as criterion II and III, the false negative rate decreased to 5.6%; however, it increases the false positive rate to 21%, so the differentiation results in channel 1 doesn't have a sufficient balance between false negative and false positive rates.

Using $\varepsilon_{10,2}$, $\varepsilon_{8,2}$, $\varepsilon_{6,2}$ and in Figure 2.4(a) had limitations in further improving the separation results. Some dots that cannot be separated by $\varepsilon_{10,2}$ or $\varepsilon_{8,2}$ but can be separated by $\varepsilon_{9,1}$ and $\varepsilon_{7,1}$. More mechanical alternation of the cells during constriction channels can bring variations in the cells' velocity profiles.

Differentiation criteria

To better define how normal cells and cancer cells can be differentiated in channel 3, specific criteria are established for separating the different cells based on their velocity profiles and their cell shape changes. Video observations revealed that MDA-MB 231 cells deformed faster than MCF-10A cells. In channel 3, MDA-MB-231 cells recovered their normal spherical shape while in the first and second relaxation regions; in contrast, here, MCF-10A tended to maintain the flattened shape they had acquired while passing through the constriction channels. When MDA-MB-231 cells continued deforming in the third and fourth constriction regions, by virtue of maintaining their flattened shape, MCF-10A cells had a smoother entry and transit in the fourth and fifth constriction regions. We propose that these differences in cell shape recovery are reflective of differing mechanical properties and these contribute to the cell separation seen in the scatter plot of MDA-MB-231 and MCF-10A cells in channel 3, shown in Figure 2.4(e). By using

the velocity at the last constriction channel and the first constriction channel we can differentiate the majority of the cancer cells from normal cells. Based on Figure 2.4(f), further decreasing of the overlapping areas between the MDA-MB-231 and MCF-10A cells can be achieved by adding the additional criteria of $\varepsilon_{7,1} < 2$. In channel 3, the entrance time of cancer cells into the fourth and fifth channel will take longer than the normal cells. Therefore, the $\varepsilon_{7,1}$ of normal cells will be larger than cancer cells. According to our experiments in channel 3, most MCF-10A cells have $\varepsilon_{7,1} > 2$, or $V7 > 3 \cdot V1$. In summary, we can further distinguish the contrasting mechanical properties between MDA-MB-231 and MCF-10A using the following criteria:

(1) Criterion I:

$$\begin{cases} \varepsilon_{10,2} = \dfrac{V_{10} - V_2}{V_2} \geq 0 \text{ (Normal cell)} \\ \varepsilon_{10,2} = \dfrac{V_{10} - V_2}{V_2} < 0 \text{ (Cancer cell)} \end{cases}$$

(2) Criterion II:

$$\begin{cases} \varepsilon_{10,2} = \dfrac{V_{10} - V_2}{V_2} \geq 0 \text{ (Normal cell)} \\ \varepsilon_{10,2} = \dfrac{V_{10} - V_2}{V_2} < 0 \text{ (Cancer cell)} \\ \varepsilon_{9,1} = \dfrac{V_9 - V_1}{V_1} \geq 2 \text{ (Normal cell)} \\ \varepsilon_{9,1} = \dfrac{V_9 - V_1}{V_1} < 2 \text{ (Cancer cell)} \end{cases}$$

(3) Criterion III:

$$\begin{cases} \varepsilon_{8,2} = \dfrac{V_8 - V_2}{V_2} \geq 0 \text{ (Normal cell)} \\ \varepsilon_{8,2} = \dfrac{V_8 - V_2}{V_2} < 0 \text{ (Cancer cell)} \\ \varepsilon_{7,1} = \dfrac{V_7 - V_1}{V_1} \geq 2 \text{ (Normal cell)} \\ \varepsilon_{7,1} = \dfrac{V_7 - V_1}{V_1} < 2 \text{ (Cancer cell)} \end{cases}$$

In order to evaluate the sensitivity of the criteria we listed, the receiver operating characteristic (ROC) curve was plotted in Figure 2.5. The sensitivities of cancer cells in channel

1, 2, and 3 were 0.69, 0.80, and 0.90, respectively; and the sensitivities of normal cells in channel 1, 2, and 3 were 0.76, 0.86, and 0.96, respectively. For channel 3 (green and purple) using criteria II & III listed above had the best differentiation results between cancer cells and normal cells.

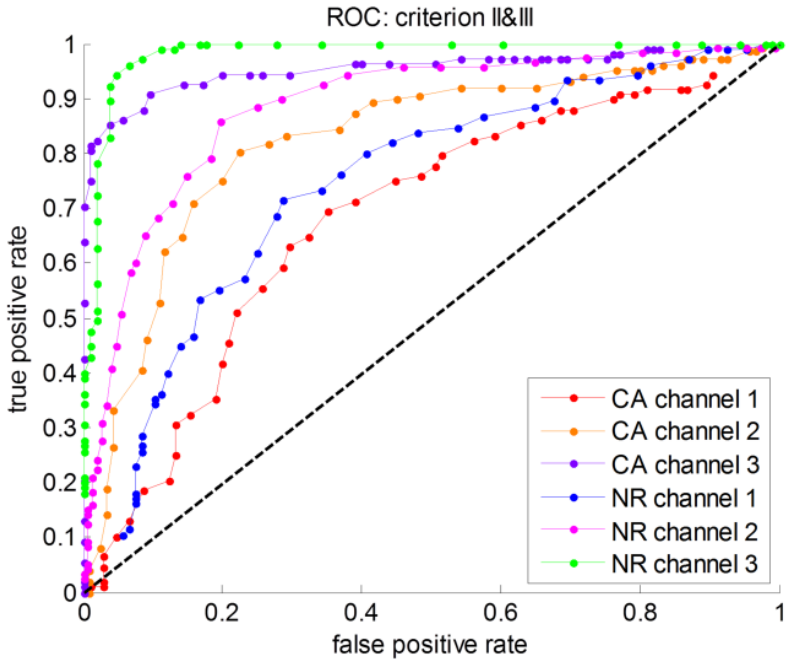

Figure 2.5: ROC curve of the cancer cells (CA) and normal cells (NR) in channel 1, 2 and 3, respectively.

Based on these differentiation criteria, scatter plots using criteria II, III, and the combination of both II & III was shown in Figure 2.6. Criteria I was able to differentiate all the normal cells (purple dots with $\varepsilon_{10,2} < 0$). After labeling the dot of each cancer cell with sequence number 1~108 in scatter plot, we observed the sequence number of each cell. Criteria II with an additional term $\varepsilon_{9,1}$ was able to identify more cancer cells with $\varepsilon_{10,2} > 0$. Criteria III was similar to criteria II, except that we only used $\varepsilon_{8,2}$ and $\varepsilon_{7,1}$. Criteria III had some overlap of normal cells in $\varepsilon_{8,2} < 0$ and $\varepsilon_{7,1} < 2$. Therefore, we combined criteria II and III together, and used scatter plots, displayed in Figure 2.6(c), to help visualize the separation. The normal cells (purple dots) were further apart to the cancer cells (green dots).

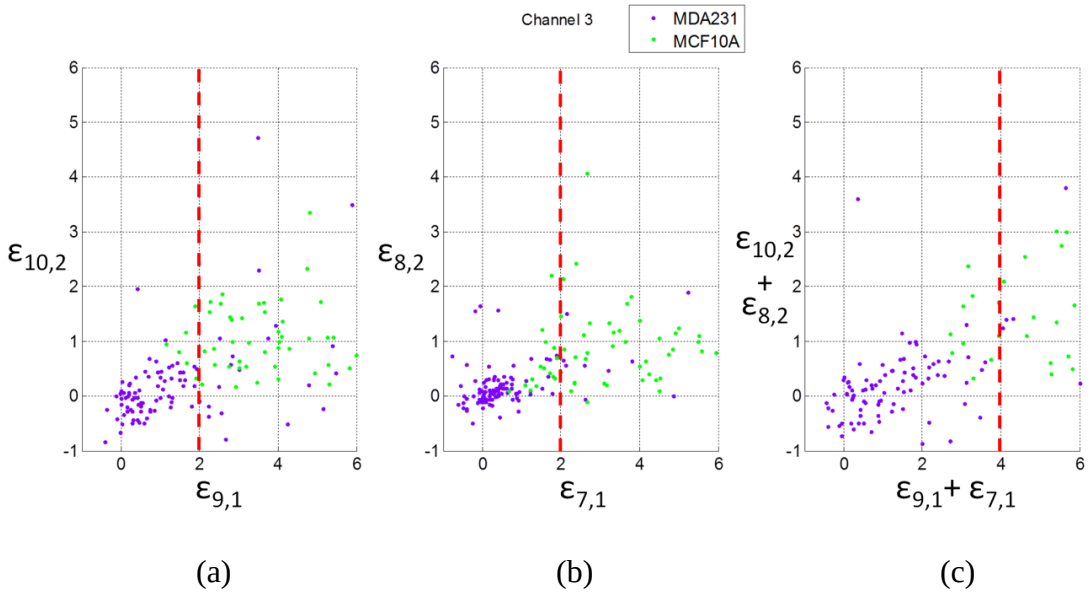

Figure 2.6: Scatter plot of using criteria II (a), III (b), and combining II & III (c) to differentiate MDA-MB-231 cells and MCF-10A cells in channel 3.

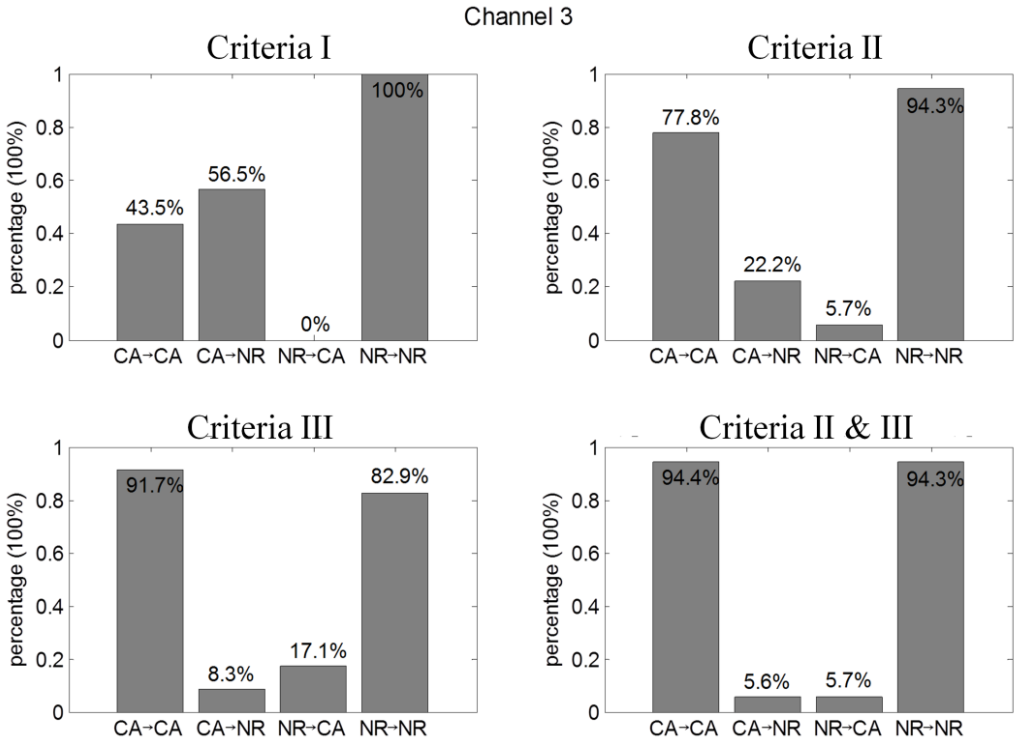

Figure 2.7: Differentiate rate of cancer cells (CA) and normal cells (NR) in channel 3 using different velocity analysis criteria.

By directly applying $\varepsilon_{10,2} > 0$, based on the scatter plot data in Figure 2.6(a) and bars in Figure 2.6(a), all of the normal cells can be recognized as normal cells (recorded as NR→NR); however, ~51% of the cancer cells were observed as normal cells (recorded as CA→NR) with $\varepsilon_{10,2} > 0$. Using criteria II and III, as shown in the scatter plot in Figure 2.6(a) and 2.6(b) and bars in Figure 2.7(b) and 2.6(c), the identification of normal cells were compromised in order to achieve higher likelihood of cancer cells being observed as either cancer cells (recorded as CA→CA) or as normal cells (CA→NR). After we applied both criteria II and III together, we achieved an acceptable ratio to differentiate cancer cells and normal cells.

Testing sample in Channel 3

In order to verify the quality of our differentiation criteria, four blind samples with either cancer cells or normal cells were tested. The data of velocity at each constriction increment in channel 3 was analyzed.

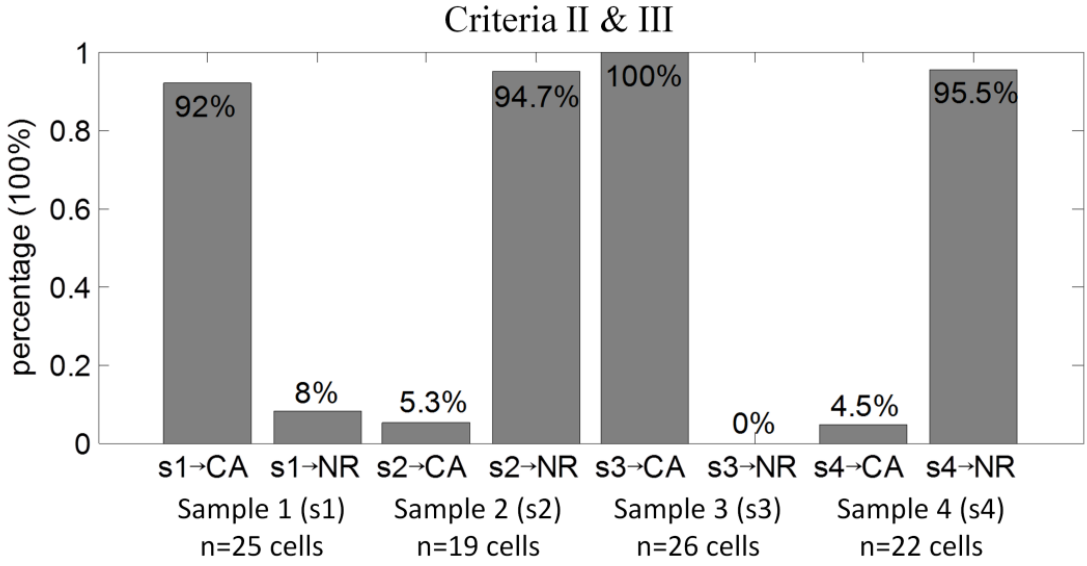

Figure 2.8: Differentiation ratio of cancer cells (CA) and normal cells (NR) using four blind-testing samples (s1, s2, s3, and s4) in channel 3.

The combination of criteria II & III was applied here to the blind-test samples (s1, s2, s3, and s4). As a result indicated in Figure 2.8, two samples were observed as cancer cells and the

other two samples were observed as normal cells, which agreed to the predicted cells before testing.

2.5 Discussion

The initial deformation of the cells was affected by the mechanical properties of the cells, since the microfluidic channel geometries and experimental conditions were the same. The kinetic behaviors of the cells were directly related to the mechanical properties, such as Young's modulus, cell membrane stiffness, and tension stress of the membrane. These velocity profiles vary between normal cells and cancer cells, because cancer cells have lower membrane stiffness and cytoskeleton strength as documented by previous studies [3, 4, 39, 40]. The velocity of the cells depends on fluidic pressure, flow rate, and the geometry of the cells. The cross-section of the microfluidic channels and flow rate are kept constant for both MDA-MB-231 and MCF-10A medium, so that the Reynolds number of both samples can be considered constant. The mechanical characteristics can be revealed by the dynamic behaviors of the cells. The stiffness of the cell membrane dominates the shear force and shear stress between the cell membrane and the microfluidic channel side wall. The Young's modulus of the cells affects the deformation of the cell membrane when the cross-section of the microfluidic channel changes. Both the stiffness of the cell membrane and the Young's modulus of the cells are typical bio-markers used to distinguish cancer cells from normal cells. By studying the average velocity at each segment and the velocity difference between different segments, we can differentiate the different cell types due to their different mechanical characteristics.

The first approaches that used microfluidics for differentiating cells were explored by using a single constriction channel like the channel 1 we presented in our device. The cells experienced a one-time deformation in a single constriction channel, which relied on both the cell size and

stiffness. The differentiation merely based on velocity was not reliable due to the variability in cell size which is unavoidable due to at a minimum, cell cycle phase dependent variations in cell size. In a single constriction channel (channel 1), our experiments had a differential ratio of 52.9% for the cancer cells, which was similar to the results of others' experiments with single constriction channel with 8 μm × 8 μm cross-section [18]. Chen, et al., used the elongation and transit time of the cells in single constriction channel to characterize breast cancer cells, with a differential ratio about 57.5% [18]. This low recognition rate was another reason why scientists were encouraged to search for new methods to further differentiate different types of cells. Rather than adding electrodes to measure impedance to combine biomechanical and bioelectrical parameters of the cells, we opted to add relaxation regions to separate the single constriction channel into multiple constriction channels to emphasize the biomechanical characteristics of the cells. Our differential ratio for both cancer cells and normal cells can reach more than 94%, which was also verified by four blind-testing samples.

From viewing images from the video microscopy, each cell, even within a cell line population, is different and unique. In the single-constriction channel (channel 1), the MDA-MB-231 cells have a higher velocity than the MCF-10A cells. The single-constriction channel with length of 250 μm was separated into 10 segments; however, the 10 segments of the velocity profiles in channel 3 included 5 velocities deformation regions. The two types of cells performed differently in velocity profiles with the five deformation regions, which was suitable in cell type differentiation. In channel 2, both cell types have a decreasing velocity at the relaxation region between 125~150 μm. In channel 3, due to the short constriction region and short relaxation region, MDA-MB-231 cells do not experience a full shape recovery process (deformation performance). Compared to channel 1, channel 3 distinguishes cell types by adding multiple deformation and

relaxation regions, which make V7, V5, V3 more useful in differentiating different cell types. Channel 3 introduced more mechanical alternations for the cells, which increases the membrane mechanical differences between normal cells and cancer cells. Each time the cell deforms, a greater separation is obtained for cells of different metastatic potential. Therefore, based on the velocity profiles generated in constriction regions and relaxation regions, channel 3 had more opportunities to have varying velocity profiles, including velocity increments, for MDA-MB-231 cells and MCF-10A cells. MCF-10A cells in channel 3 have a long deformation time at the entrance, however, they kept the rod-like shape and moved into the succeeding constriction regions with a higher initial velocity. With the continuous acceleration, MCF-10A cells reach a higher final velocity than MDA-MB-231 cells. In other words, once the MCF-10A cells deform, they retain the shape that facilitates their passage. MDA-MB-231 cells show more plasticity in their shape with a net retardation of their velocities.

In our experiments, the effect of multiple relaxation regions are studied in multiple-constriction channels (channel 3) in order to differentiate between cancer cells and normal cells. In future work, the length of relaxation regions can be modified and tested. The cancer cells and normal cells behave differently during the constriction and relaxation regions. The constriction time was determined by the constriction channel length, while the relaxation time was determined by relaxation position and relaxation length. With a longer relaxation region, the cancer cells can recover more after the constriction channels, which may have a recovery that behaves differently compared to the recovered normal cells.

2.6 Conclusions

After calculating the velocity increments in the fourth channel and fifth channel compared to the initial velocity in multiple-constriction channels (channel 3), the scatter plot of the single

cell velocity data of each MDA-MB-231 (n= 108 cells) and MCF-10A (n= 105 cells) cells showed clear separation of the two cell lines into distinct regions, which successfully differentiated ~94.4% of the cancer cells from normal cells. Due to the fact that normal cells are stiffer than cancer cells, multiple relaxation regions gave cancer cells more chance to recover into its original shape, and enlarged the dynamic velocity increments along the constriction channels. Our measurement by smart phone video through microscope was reliable. Furthermore, this method has a potential to be developed into a convenient phone application of health examination. Our experimental results indicated that multi-constriction microfluidic channels can be used to differentiate metastatic MDA-MB-231 and MCF-10A cells at the single cell level. For future studies, the quantity of parallel constriction channels can be increased to have higher throughput.

References

1. Nagrath, S., et al., Isolation of rare circulating tumour cells in cancer patients by microchip technology. Nature, 2007. **450**(7173): p. 1235-1239.
2. Xue, C., et al., Constriction channel based single-cell mechanical property characterization. Micromachines, 2015. **6**(11): p. 1794-1804.
3. Babahosseini, H., J.S. Strobl, and M. Agah, Single cell metastatic phenotyping using pulsed nanomechanical indentations. Nanotechnology, 2015. **26**(35): p. 354004.
4. Nikkhah, M., et al., The cytoskeletal organization of breast carcinoma and fibroblast cells inside three dimensional (3-D) isotropic silicon microstructures. Biomaterials, 2010. **31**(16): p. 4552-4561.
5. Zhang, J., W. Sheng, and Z.H. Fan, An ensemble of aptamers and antibodies for multivalent capture of cancer cells. Chemical Communications, 2014. **50**(51): p. 6722-6725.
6. Zhang, J. and Z.H. Fan, A universal tumor cell isolation method enabled by fibrin-coated microchannels. Analyst, 2016. **141**(2): p. 563-566.
7. Riethdorf, S., et al., Detection of circulating tumor cells in peripheral blood of patients with metastatic breast cancer: a validation study of the CellSearch system. Clinical Cancer Research, 2007. **13**(3): p. 920-928.
8. Zabaglo, L., et al., Cell filtration-laser scanning cytometry for the characterisation of circulating breast cancer cells. Cytometry Part A, 2003. **55**(2): p. 102-108.
9. Juratli, M.A., et al., Real-time monitoring of circulating tumor cell release during tumor manipulation using in vivo photoacoustic and fluorescent flow cytometry. Head & neck, 2014. **36**(8): p. 1207-1215.
10. Cruz, I., et al., Evaluation of multiparameter flow cytometry for the detection of breast cancer tumor cells in blood samples. American journal of clinical pathology, 2005. **123**(1): p. 66-74.
11. Bagnall, J.S., et al., Deformability of tumor cells versus blood cells. Scientific reports, 2015. **5**.
12. Zheng, S., et al., 3D microfilter device for viable circulating tumor cell (CTC) enrichment from blood. Biomedical microdevices, 2011. **13**(1): p. 203-213.
13. Mohamed, H., et al., Development of a rare cell fractionation device: application for cancer detection. IEEE transactions on nanobioscience, 2004. **3**(4): p. 251-256.
14. Sarioglu, A.F., et al., A microfluidic device for label-free, physical capture of circulating tumor cell clusters. Nature methods, 2015. **12**(7): p. 685-691.
15. Riahi, R., et al., A novel microchannel-based device to capture and analyze circulating tumor cells (CTCs) of breast cancer. International journal of oncology, 2014. **44**(6): p. 1870-1878.
16. Lee, A., et al., All-in-one centrifugal microfluidic device for size-selective circulating tumor cell isolation with high purity. Analytical chemistry, 2014. **86**(22): p. 11349-11356.
17. Loutherback, K., et al., Deterministic separation of cancer cells from blood at 10 mL/min. AIP advances, 2012. **2**(4): p. 042107.
18. Chen, J., et al., Classification of cell types using a microfluidic device for mechanical and electrical measurement on single cells. Lab on a Chip, 2011. **11**(18): p. 3174-3181.
19. Zhao, Y., et al., Single-Cell Electrical Phenotyping Enabling the Classification of Mouse Tumor Samples. Scientific reports, 2016. **6**.
20. Huang, S.-B., et al., A clogging-free microfluidic platform with an incorporated pneumatically driven membrane-based active valve enabling specific membrane capacitance and

cytoplasm conductivity characterization of single cells. Sensors and Actuators B: Chemical, 2014. **190**: p. 928-936.

21. Huang, S.-B., et al., Classification of cells with membrane staining and/or fixation based on cellular specific membrane capacitance and cytoplasm conductivity. Micromachines, 2015. **6**(2): p. 163-171.

22. Zhao, Y., et al., Simultaneous characterization of instantaneous Young's modulus and specific membrane capacitance of single cells using a microfluidic system. Sensors, 2015. **15**(2): p. 2763-2773.

23. Hou, H.W., et al., Deformability study of breast cancer cells using microfluidics. Biomedical microdevices, 2009. **11**(3): p. 557-564.

24. Mak, M., C.A. Reinhart-King, and D. Erickson, Elucidating mechanical transition effects of invading cancer cells with a subnucleus-scaled microfluidic serial dimensional modulation device. Lab on a Chip, 2013. **13**(3): p. 340-348.

25. Jin, D., et al., A microfluidic device enabling high-efficiency single cell trapping. Biomicrofluidics, 2015. **9**(1): p. 014101.

26. Guan, G., et al., Real-time control of a microfluidic channel for size-independent deformability cytometry. Journal of Micromechanics and Microengineering, 2012. **22**(10): p. 105037.

27. Hoffman, B.D., C. Grashoff, and M.A. Schwartz, Dynamic molecular processes mediate cellular mechanotransduction. Nature, 2011. **475**(7356): p. 316-323.

28. Zheng, Y., et al., Recent advances in microfluidic techniques for single-cell biophysical characterization. Lab on a Chip, 2013. **13**(13): p. 2464-2483.

29. Khan, Z. and S. Vanapalli, Probing the mechanical properties of brain cancer cells using a microfluidic cell squeezer device. Biomicrofluidics, 2013. **7**(1): p. 011806.

30. Bagnall, J.S., et al., Deformability-based cell selection with downstream immunofluorescence analysis. Integrative Biology, 2016. **8**(5): p. 654-664.

31. Luo, Y., et al., A constriction channel based microfluidic system enabling continuous characterization of cellular instantaneous Young's modulus. Sensors and Actuators B: Chemical, 2014. **202**: p. 1183-1189.

32. Zhao, Y., et al., A microfluidic system enabling continuous characterization of specific membrane capacitance and cytoplasm conductivity of single cells in suspension. Biosensors and Bioelectronics, 2013. **43**: p. 304-307.

33. Chen, J., et al., Electrodeformation for single cell mechanical characterization. Journal of Micromechanics and Microengineering, 2011. **21**(5): p. 054012.

34. Adamo, A., et al., Microfluidics-based assessment of cell deformability. Analytical chemistry, 2012. **84**(15): p. 6438-6443.

35. Byun, S., et al., Characterizing deformability and surface friction of cancer cells. Proceedings of the National Academy of Sciences, 2013. **110**(19): p. 7580-7585.

36. Liu, Z., et al., High throughput capture of circulating tumor cells using an integrated microfluidic system. Biosensors and Bioelectronics, 2013. **47**: p. 113-119.

37. Wang, Y., et al., In situ simultaneous monitoring of ATP and GTP using a graphene oxide nanosheet–based sensing platform in living cells. Nature protocols, 2014. **9**(8): p. 1944-1955.

38. Chen, J., J. Li, and Y. Sun, Microfluidic approaches for cancer cell detection, characterization, and separation. Lab on a Chip, 2012. **12**(10): p. 1753-1767.

39. Babahosseini, H., et al., Sub-cellular force microscopy in single normal and cancer cells. Biochemical and biophysical research communications, 2015. **463**(4): p. 587-592.

40. Carmichael, B., et al., The fractional viscoelastic response of human breast tissue cells. Physical biology, 2015. **12**(4): p. 046001.
41. Ren, X., Ghassemi, P., Babahosseini, H., Strobl, J. S., & Agah, M., Single-Cell Mechanical Characteristics Analyzed by Multiconstriction Microfluidic Channels. ACS Sensors, 2017. **2**(2), p. 290-299.

3. Bioimpedance Detection of Transit Time

3.1 Introduction

Cells deform as they pass through microfluidic constriction channels. Cell deformation time (entry time) and cell passage velocity through a constriction channel relating to cell viscoelastic properties have been used as biomechanical markers to differentiate between normal and diseased cells, and to analyze the efficacy of therapeutic drugs [1, 2]. Cell velocities measured in constriction channels can be used to characterize single cells and even to differentiate between cells of different metastatic potential [3]. The common practice is to use video microscopy to image cell movements in channels and to perform advanced post-processing image analysis, both of which limits the system throughput and clinical applicability [3]. Impedance spectroscopy alleviates the aforementioned limitations and also provides further insight into cell bioelectrical properties. Bioelectrical signatures, such as specific membrane capacitance and cytoplasm conductivities, give another dimension to characterize and distinguish different cells. This chapter introduces two microfluidic deformability bioimpedance sensing devices, Multi-Electrode Single Channel (MESC) chip and Single Electrode Multi-Channel (SEMC) chip, which attempt to improve resolution of velocity measurements and throughput, respectively. MESC consists of a single deformation channel with an array of electrodes, while SEMC is made up of an array of parallel deformation channels with a single pair of electrodes.

3.2 Materials and Methods

Cell Culture

For experimentation we used the highly metastatic breast cancer cell-line MDA-MB-231 (American Type Culture Collection (ATCC), Manassas, VA). To prepare the samples, the MDA-MB-231 cells are detached from a culture flask using 0.5 mL of trypsin-EDTA (1X) and 2 minutes

of trypsinization at 37°C. The detached cells are then suspended in culture medium and diluted to ~10×10^4 cells/mL. During experimentation, samples are stored at 37°C in order to maintain the ideal cell environment. Cell viability is then tested using trypan blue (trypan blue solution (0.4%), lot 42K2360, Sigma), and the cells were determined to be 100% viable.

Device Fabrication

Fabrication of the electrodes starts with the patterning of a Pyrex wafer with photoresist (S1813, MicroChem, Newton, MA) by means of photolithography. MESC electrodes are made of Indium Tin Oxide (ITO), while SEMC electrodes are gold. Using sputter deposition, ITO electrodes are evaporated onto the patterned pyrex wafer and created using typical lift-off techniques for MESC. SEMC uses the same method, except gold electrodes are evaporation on the pyrex substrate using electron beam (e-beam) evaporation. To create the microfluidic channels, we patterned a silicon wafer with two layers of SU-8 (SU-8 3005 and SU-8 3025, MicroChem, Newton, MA) through photolithography to create a master mold. The SU-8 3005 was used to build the constriction channels with a height of 8 μm; and the SU-8 3025 was used to build the remaining microfluidic channels with a total height of ~30 μm. The mold is then coated with tridecafluoro-1,1,2,2-tetrahydrooctyl-1-tricholosilane (TFOCS, Fisher Scientific) for easy release of polydimethylsiloxane (PDMS). Using soft-lithography techniques, we use the master mold to create the PDMS microchannel. Through plasma activated bonding we align and bond the PDMS microchannels onto the glass with electrodes. Due to misalignment and channel clogging the device yield is 80%. Each electrode has its own bond pad so that wires can be soldered in order to be connected to the impedance spectroscope.

3.3 MESC Device

Channel Design and Experimental Setup

The sensor consists of two separate channels, delivery and constriction, to prevent cell accumulation at the constriction and prohibits clogging (shown in Figure 3.1).

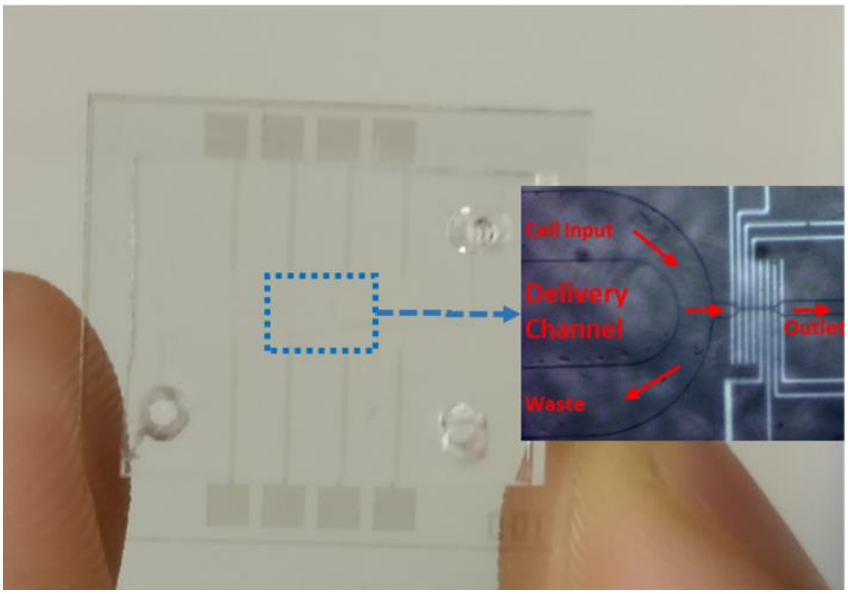

Figure 3.1: Full view of microfluidic biosensor.

The delivery channel consists of single cells suspended in a medium that pass through the channel from an inlet to an outlet. Once the cells are inputted at the inlet, a vacuum pump is used to apply a negative pressure at the outlet, which allows the cells to flow through the delivery channel because of the pressure differences. The entrance of the constriction channel is located at the center of the delivery channel. A negative pressure is being applied at the end of the constriction channel via a Harvard Apparatus syringe pump in order to initiate flow through the constriction channel. Once a cell has entered the constriction channel, the flow coming from the delivery channel stops until the cell trapped in the constriction channel has passed through completely.

The device (Figure 3.1) consists of an array of eight 10 µm-wide electrodes with 10 µm spacing between each electrode (Figure 3.2). The purpose of implementing ITO electrodes was to achieve an all-transparent device that can be used to fully track cells from the entrance to the exit of the constriction channel using an inverted microscope (Zeiss Axio Observer, LSM-510, Thornwood, NY); the transparent electrodes cover half of the channel. The outermost electrodes are aligned 15µm away from the entrance and exit of the 100 µm-long, 8 µm-wide and deep constriction channel. Electrode #1 or 'E1' and Electrode #8 (E8) are located at the entrance and exit, respectively, of the constriction channel.

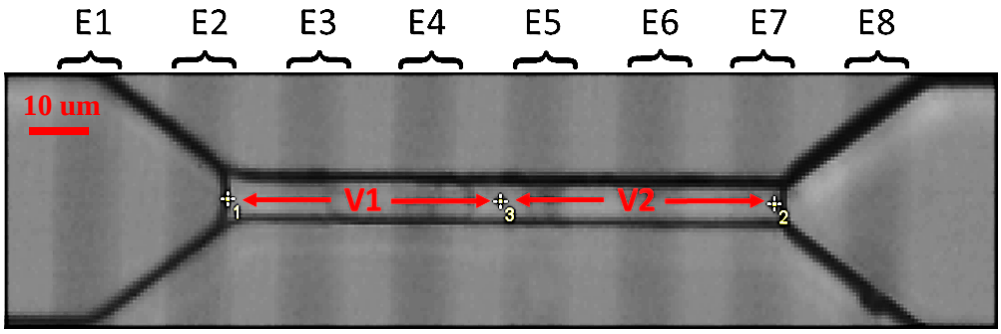

Figure 3.2: Electrode array. V1 and V2 represents velocity in the 1st and 2nd 50um of the channel, respectively.

Experimentation was done using a multitude of electrode-pair combinations (listed in Table 3.1) by applying a 2V AC signal at 8 different frequencies, ranging from 1~1000 kHz, while measuring the impedance between each pair of electrodes. Each configuration was tested pairwise both simultaneously and individually. For example for configuration [A], impedance was measured across Pair 1 and Pair 2 individually, then measured simultaneously. Measurements were taken at a high sampling rate, which allowed us to have a high enough resolution to track the cell at specific positions and in turn obtain accurate velocity measurements. The purpose of taking these measurements was to see how simultaneous impedance measurements affect each other.

High-speed video recording, at 500 frames per second (FPS), was done for cross verification of cell location and impedance signals.

Table 3.1: Electrode configurations.

Configuration	Pair 1	Pair 2
[A]	E1→E2	E7→E8
[B]	E2→E5	E4→E7
[C]	E2→E7	E4→E5
[D]	E2→E4	E5→E7

Results/Discussion

With the array of eight electrodes (Figure 3.2) we were able to explore multiple electrode configurations (Table 3.1) for tracking the transit of cancer cells through the constriction channel. All configurations provided interesting data, but each provided varying types of information. The variations in the obtained impedance data were related to the sensitivity and overall tracking capabilities. For instance, whether or not the electrode pair can track the cell from entrance to exit or only as it passes through a certain region in the constriction channel. Some configurations provided lower sensitivities and redundant information about the cells, so these combinations were discarded. Using the Zurich Instrument Spectroscope, we were able to measure two pairs of electrodes simultaneously, allowing us to capture two different types of measurements. For example, the combination of E1→E8 and E4→E5, where one electrode pair gave information about the cell's transit throughout the whole channel and the other a higher resolution measurement of the cell's transit through the center of the channel, respectively. Configuration [A] gave us

information about the complete transit of the cell, where Pair 1 and Pair 2 were used as secondary confirmations of each other. Configuration [B] was measured in hopes of obtaining differential measurements, but simultaneous measurements using this electrode pair resulted in each pair interfering with each other, greatly reducing the sensitivity and loss of the accurate cell tracking. Configurations [C] and [D] also resulted in loss of important information due to measurement interference. This interference was likely due to the electric field that each electrode pair generates, so electrode pairs within close proximity of each other experience some sort of interference making the resulting impedance measurement very noisy. As the signal to noise ratio was greatly decreased, it was difficult to distinguish between variations in the impedance plots due to cell transitions or noise.

We used MDA-MB-231 cells, highly metastatic breast cancer cells, in this manuscript because they are a long-established cell line typically used as a model system for preliminary experimentation. Figure 3.3 displays the movement of a deformed cell inside the constriction at different important points of the cell's transit. These meaningful points are listed in Table 3.2 and were selected because they provided meaningful information regarding the tracking of cells and measuring velocities at in the first and second half of the constriction channel.

Table 3.2: Cell position with corresponding description.

Position	Description
[1]	Cell reaches entrance.
[2]	Cell completely enters channel.
[3]	Front of cell reaches channel center.
[4]	Back of cell reaches channel center.
[5]	Front of cell reaches channel exit.
[6]	Cell completely exits channel.

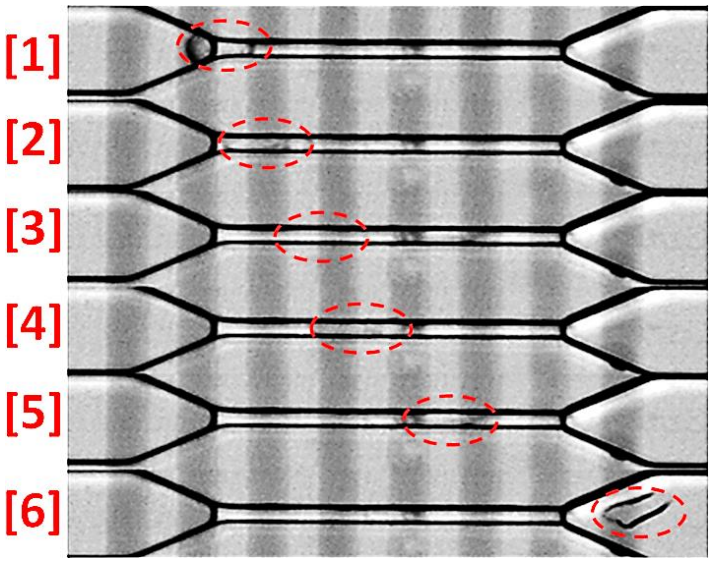

Figure 3.3: Figures of cell position as described in Table 3.2.

For this paper, we focused on the configuration where E1→E2 and E7→E8 are Pair 1 and Pair 2, respectively, and are being measured simultaneously. Velocity in the first (V1) and second (V2) half of the constriction channels (shown in Figure 3.2) and the entry and transit times were measured, all of which can give us information about the biomechanical properties of the cell. Figure 3.4 shows the transient impedance changes corresponding with cell locations (numbers in red corresponding to Table 3.2) which occur during a 74.5 sec transit of a cell. Significant changes in impedance slopes marked key events during cell transition. For instance, when a cell reaches the entry point, the impedance suddenly increases in Pair 2 as the current is blocked. Also, when the entire cell deforms and enters the channel, the impedance on Pair 2 starts to increase until it passes the channel center. Using the precise locations of the cells, cell velocity for the first/second half of the constriction channel was determined.

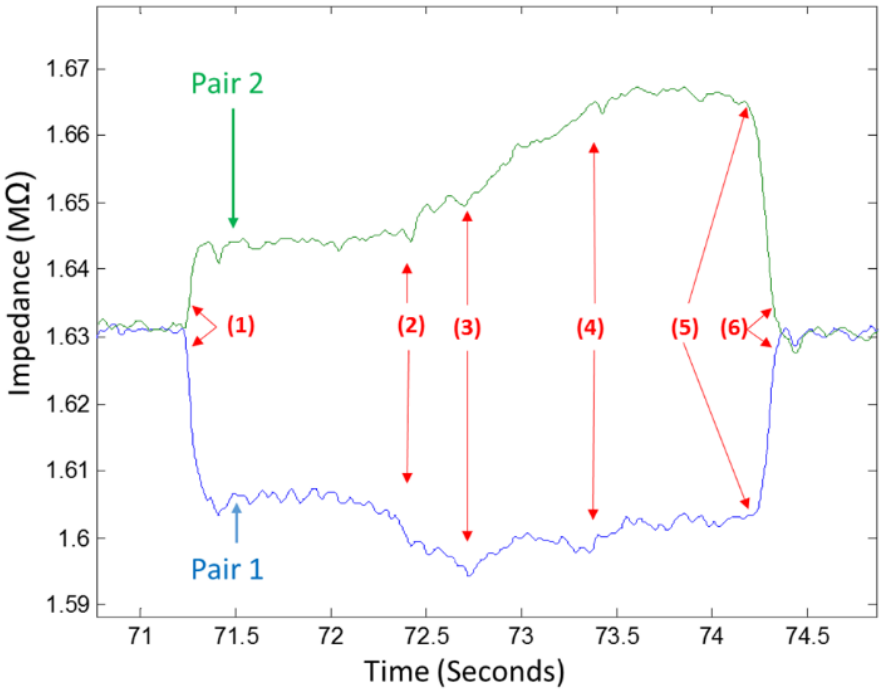

Figure 3.4: Plot of a single cell passing through constriction channel using Configuration A. Points 1-6 correspond to channel locations mentioned in Figure 3.3.

To calculate the velocity using the high-speed recorded video we used formulas (1) and (2) shown below:

$$\textbf{Velocity 1 (V1)} = \frac{50}{(T_{FMP} - T_{Ent})} \qquad (1)$$

$$\textbf{Velocity 2 (V2)} = \frac{50}{(T_{Ex} - T_{FMP})} \qquad (2)$$

T_{Ent} represents the time where the front of the cell reaches the entrance of the channel, T_{FMP} represents the time at which the front of the cell reaches the midpoint of the constriction channel, and T_{Ex} represents the time when the front of the cell reaches the exit.

We then compared velocity measurements using impedance plots and high-speed video (Figure 3.5). The exact velocity measurements (velocity measured from high-speed video) slightly

varies from the estimated velocity (velocity measured from the impedance plot). As you can see from Figure 3.5 the velocities are comparable which indicates that the impedance data are sufficient for measuring the approximate cell velocity as the cell transits through a constriction region. The ability to calculate the approximate cell velocity at the two different constriction regions indicates that this device can be used to measure the velocities using the impedance data. In turn, this can replace the long and intensive video analysis methods that is currently used in cell deformability assays.

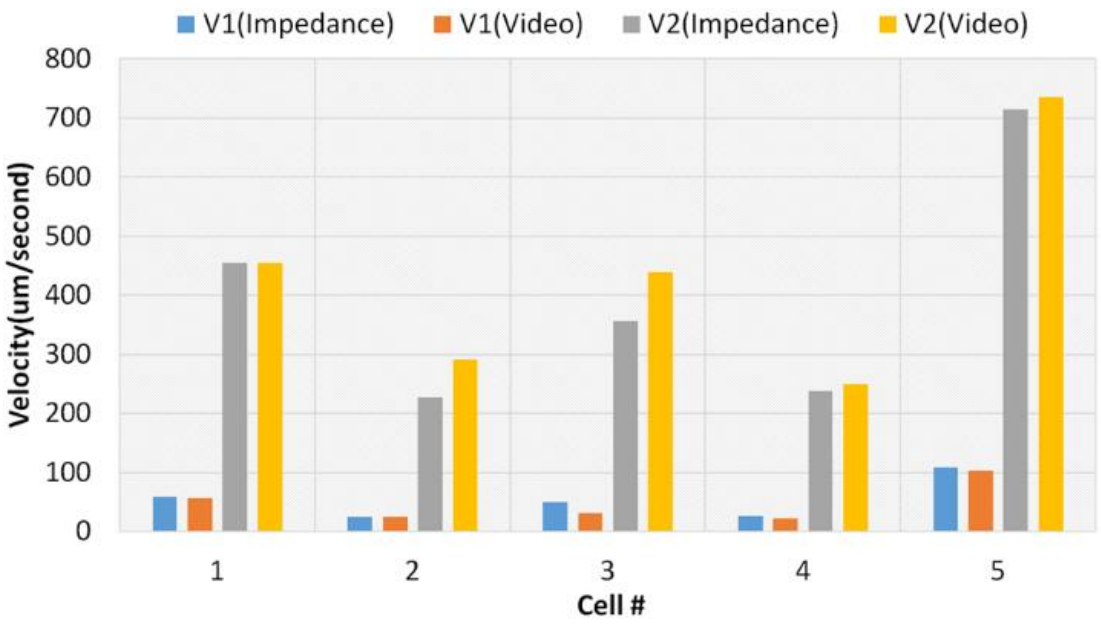

Figure 3.5: Comparison of measured cell velocity from impedance data and high-speed video. Each Cell # represents a single cell.

Between each of the six important cell location points listed in Table 3.2 and shown in Figure 3.4, there are some minor variations in the impedance. We theorize that these minor variations could be related to the location of the nucleus in the cell as it is not necessarily located in the center of the cell. This can be useful information because a cell's nucleus has different properties

compared to membrane. Our proposed chip hypothetically can provide data regarding cell/nucleus size ratio, an important indicator of cell health status [4].

3.4 SEMC Device

Channel Design and Experimental Setup

This device consists of 4 parallel deformation channels with a single electrode pair (Figure 3.6). Each deformation channel has a relaxation region in between two constriction regions. A single-cell suspension is inserted into the inlet and a positive pressure is applied using a Harvard Apparatus syringe pump. Thus, cells are forced to pass through the constriction regions towards the outlet on the other end of the device.

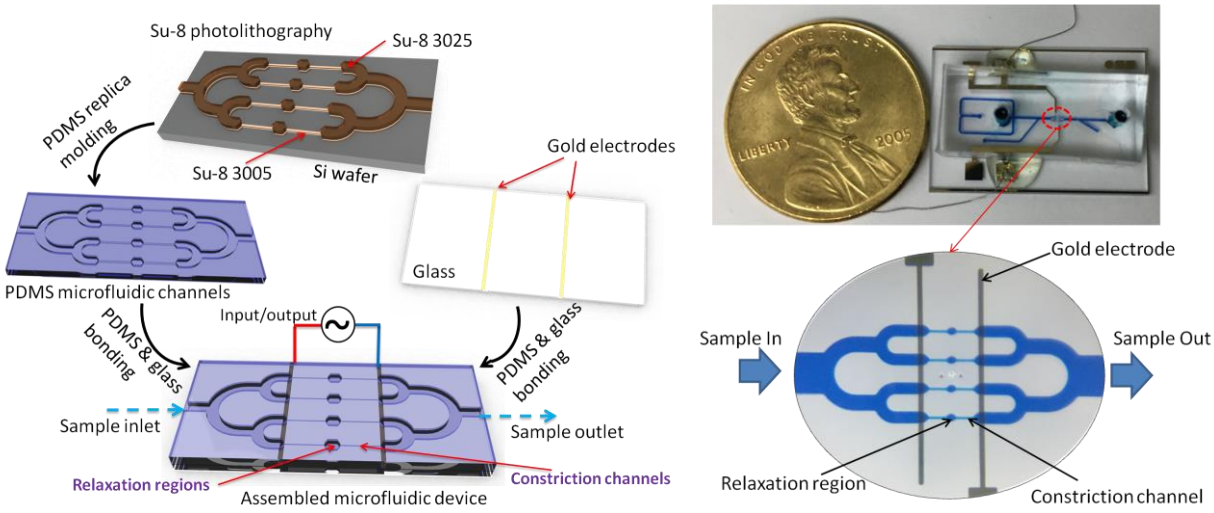

Figure 3.6: Device fabrication processes and device configurations.

The microfluidic device was mounted on an inverted microscope (Zeiss Axio Observer, LSM-510, Thornwood, NY). Video of cells traveling through the microfluidic channel was record at 240 FPS using a smartphone. The electrodes are connected to an impedance analyzer (HF2IS impedance spectroscope, Zurich Instruments, Zurich, Switzerland). Impedance measurements were taken by applying an AC signal with an amplitude of 1V on the electrodes. Data was collected at four different frequencies (1 kHz, 10 kHz, 100 kHz, and 1 MHz). Impedance results

were processed in MATLAB to find the amplitude ratio and phase shift, which are known to be major bio-signatures of cells. The amplitude ratio is defined as:

$$\text{Amplitude ratio} = \frac{Z_{\text{peak}} - Z_{\text{base-line}}}{Z_{\text{base-line}}} \qquad (3)$$

Z_{peak} represents the highest amplitude peak while the $Z_{baseline}$ represents the impedance value before the cell has entered. The phase shift represents phase difference between input AC voltage and measured AC current response. This shift exists due to the specific membrane capacitance of the cells.

Results/Discussion

The location of cancer cell #1(red) and #2(blue) in the microchannel with respect to time is plotted in Figure 3.8a. Due to the deformation channel design, the impedance profile of each cell has two peaks with a baseline in between (Figure 3.8b). The impedance measured across all four channels increased when cell #1 entered one of the four channels, impedance had maxima at t=9~13s and t=16~20 s which correlated with cell #1 location in the constriction channels (Figure 3.7). The impedance dropped sharply as cell #1 entered the relaxation region (t=14~15s); here the impedance value returned to the original baseline typical of the cell-free solution. A smaller cancer cell #2, entered another channel as cell #1 was passing through the microchannel, which was detected by the electrode pair at t=6s.

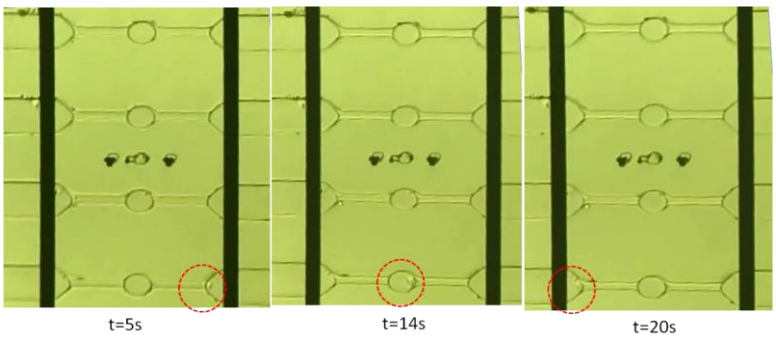

Figure 3.7: Image of the four parallel microchannels with electrodes (dark vertical bars); cancer cell #1 location (encircled in red) at 5, 14, and 20 seconds, respectively is recorded by camera.

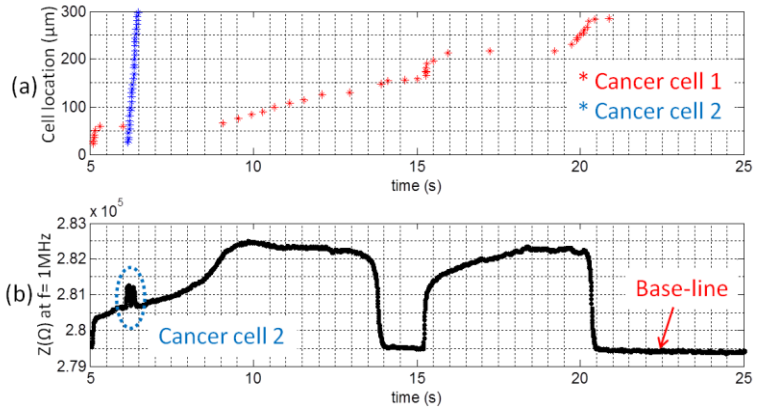

Figure 3.8: The location of the cancer cells by time (a), and the impedance measurements of the cells (b).

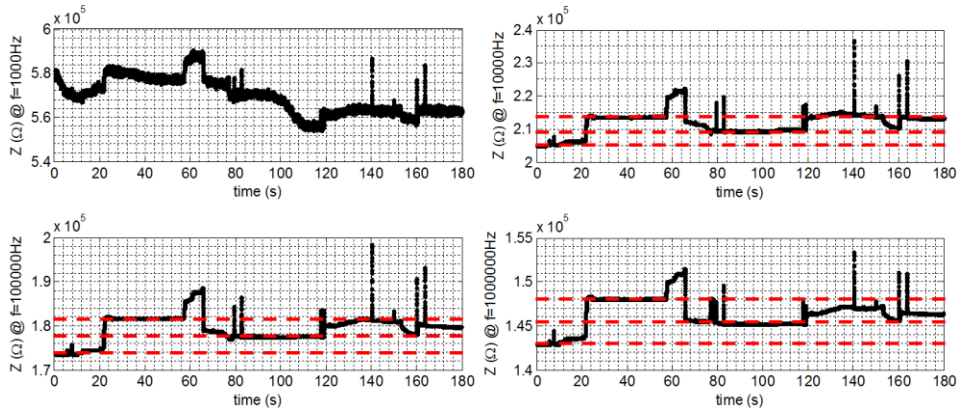

Figure 3.9: Three base-lines of the impedance measurement results of MDA-MB-231 cells at four frequencies.

The impedance measurement results of MDA-MB-231 showed three different base-lines at 10k, 100k, and 1MHz (Figure 3.8), because the cells clogged in constriction channels caused an increasing of overall impedance value. The three different base-lines showed cells were trapped in three channels. At the same time, cells passing through the fourth channel were still recorded by impedance measurement. The amplitude ratio and phase shift data of each cell was collected from the impedance measurement. They are calculated using amplitude values, and the real and imaginary parts of impedance compared to the base-line.

3.5 Conclusion and Future Impact

To summarize, we report two bioimpedance sensing devices that are each coupled with a cell deformability assay in an innovative microfluidic device for label-free analysis of single-cell biophysical properties. MESC is an all-transparent device that uses impedance sensing to track the position of a cell as it transits through a constriction channel, eliminating the need for extensive post-processing image analysis. The highly sensitive device can accurately measure transit times along with the average cell velocity at different regions of the constriction channel, which are both indicators of viscoelastic properties of the cells. SEMC can measure cell travel time along with impedance amplitude and phase shift. Measurements for up to four cells at four different frequencies can be taken accurately. The throughput of this device greatly increased compared to our previous designs.

The bio-electromechanical abilities of our devices provides implications for future research related to nuclear tracking, high-throughput applications, and drug efficacy tests. As the device can track cells with a high sensitivity, it is possible to obtain specific information on individual components of the cell, such as the size nucleus. Since the size of the nucleus can be an indicator of cell health, the device could potentially differentiate between healthy and diseased cells [4]**.** Finally, the devices can provide biomechanical and bioelectrical properties of cells, making them a potentially useful tool for drug efficacy studies [5].

References:

1. Babahosseini, H., et al., *The impact of sphingosine kinase inhibitor-loaded nanoparticles on bioelectrical and biomechanical properties of cancer cells.* Lab on a Chip, 2016. **16**(1): p. 188-198.
2. Galler, K., et al., *Making a big thing of a small cell–recent advances in single cell analysis.* Analyst, 2014. **139**(6): p. 1237-1273.
3. Ren, X., et al., *Single-cell mechanical characteristics of human breast cell lines analyzed by multi-constriction microfluidic channels*. 2017, American Association for Cancer Research.
4. Lim, C.S., et al., *Measurement of the Nucleus Area and Nucleus/Cytoplasm and Mitochondria/Nucleus Ratios in Human Colon Tissues by Dual-Colour Two-Photon Microscopy Imaging.* Scientific reports, 2015. **5**: p. 18521.
5. Ramasamy, S., D. Bennet, and S. Kim, *Drug and bioactive molecule screening based on a bioelectrical impedance cell culture platform.* International journal of nanomedicine, 2014. **9**: p. 5789.

4. Conclusion and Future Outlook

Conclusion

In this thesis, a variety of microfluidic chips were developed for label-free measurements of biomechanical and bioelectrical properties at the single-cell level. To achieve these results, there are many different skills one would need to learn. These skills include device design, microfabrication, impedance spectroscopy, soft lithography with PDMS, cell culturing, and drug treatment techniques. Chapter 1 gives a background on how cells can be modeled as biophysical objects. The chapter also discusses different methods of probing cells for their biomechanical and bioelectrical properties, in combination with impedance spectroscopy in deformability assays. Chapter 2 reports a microfluidic device consisting of multiple constriction channels with varying number of constriction counts. Biomechanical properties of breast cancer and nontumorigenic breast cells were assessed by comparing the effect of varying deformation and relaxation regions. Velocity profiles of these cells were used to distinguish between each cell type with 95% accuracy. Chapter 3 reports two microfluidic biosensors that combine impedance spectroscopy with deformability assays to alleviate extensive post-processing times. The first device, MESC, uses an array of electrodes to measure high-resolution cell velocities as they transit through the deformation region. SEMC utilizes parallel deformations channels with a pair of electrodes to improve the throughput and automate data collection of deformability assays.

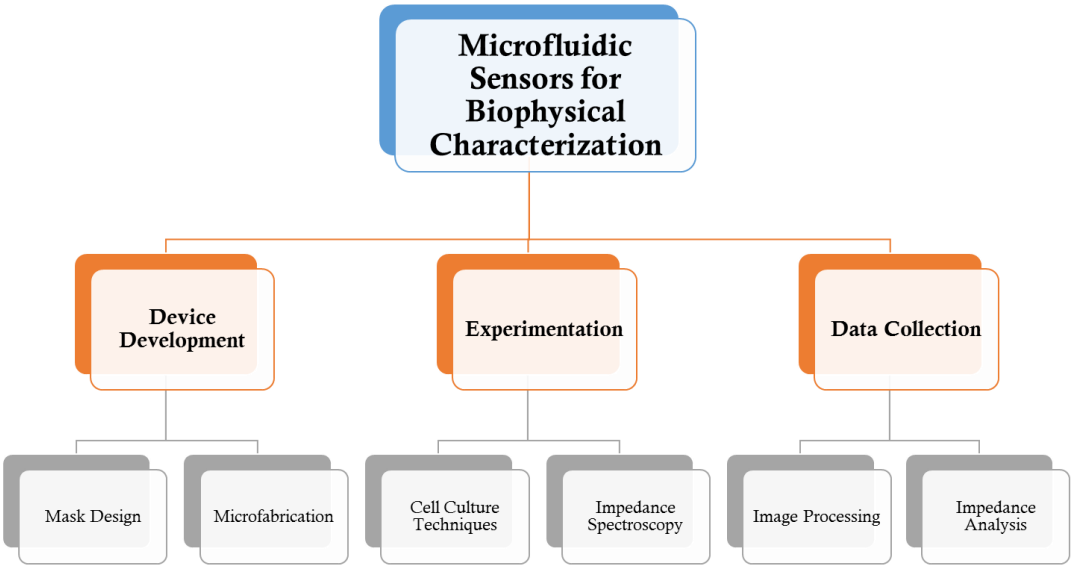

Figure 4.1: Skills necessary for creating microfluidic sensors for biophysical characterization

Future Outlook

There are a wide variety of options for future work that can build upon the current technology. Some avenues include: device improvement, device modeling, and clinical device development. Improvements that can be made on current devices include increasing throughput and resolution, and reducing noise and post-processing time. To further increase throughput, one can add more channels in parallel so that data collection can be done in many channels simultaneously. Improving resolution on velocity tracking devices can be done by adding floating electrodes inside the constriction channels which could potentially act as markers or checkpoints for when the cell crosses them. Improving resolution of device will reduce error in velocity measurements, making the device more robust. Additionally, to reduce noise we can take differential impedance measurements as the cells pass through the microfluidic channels. Modeling current devices would be an appropriate step to better understand the results of the device better. By modeling the electric field created by the electrodes could be a good method of

understanding the impedance results. It can also be important for optimizing the electrodes and optimizing the device design. Finally, the end goal of current work is to create robust devices for clinical applications. Although developing such devices for clinical applications is challenging, it is imperative for the advancement of cancer diagnostics and treatments.

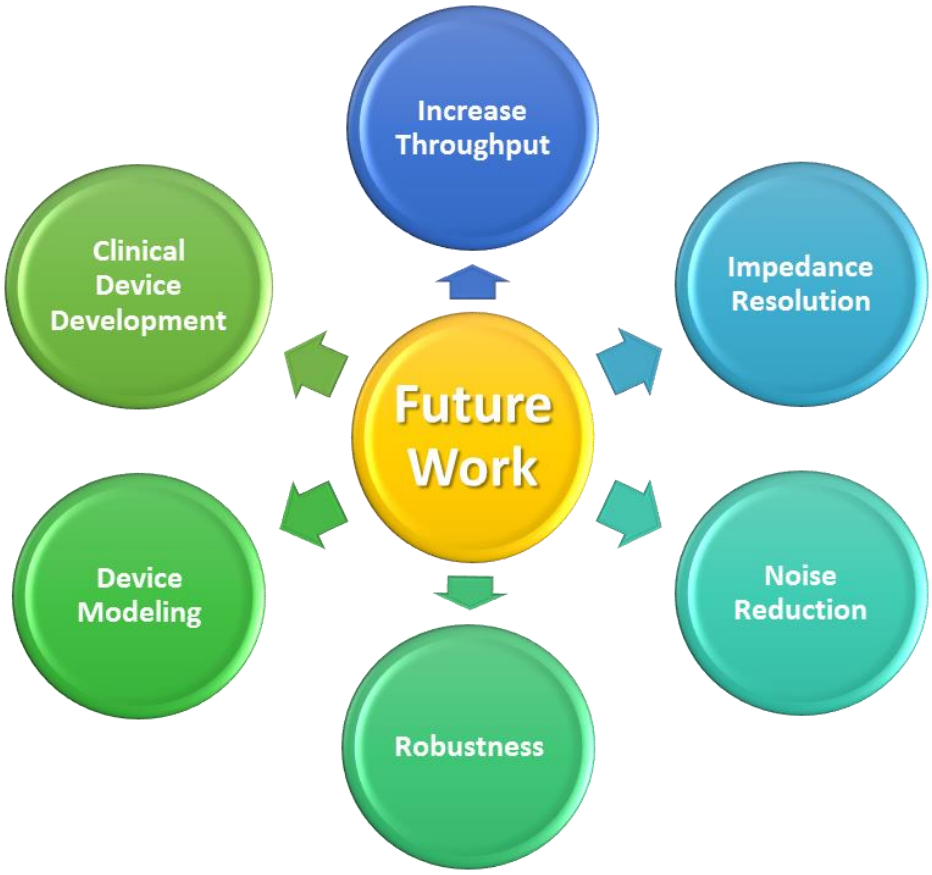

Figure 4.2: Diagram illustrating different avenues of future work.